Advances in Nano Research, *Vol. 16, No. 4 (2024) 395-412*
https://doi.org/10.12989/anr.2024.16.4.395

On vibrations of functionally graded carbon nanotube (FGCNT) nanoplates under moving load

Alaa A. Abdelrahman[1], Ismail Esen[2], Mohammed Y. Tharwan[**3], Amr Assie[3,5] and Mohamed A Eltaher[*4.5]

[1]*Mechanical Design & Production Department, Faculty of Engineering, Zagazig University, P.O. Box 44519, Zagazig, Egypt*
[2]*Department of Mechanical Engineering, Karabuk University, Karabuk, Turkey*
[3]*Mechanical Engineering Department, Faculty of Engineering, Jazan University, P. O. Box 45142, Jazan, Kingdom of Saudi Arabia*
[4]*Mechanical Engineering Department, Faculty of Engineering, King Abdulaziz University, P.O. Box 80204, Saudi Arabia*
[5]*Mechanical Design & Production Department, Faculty of Engineering, Zagazig University, P.O. Box 44519, Zagazig, Egypt*

(*Received June 8, 2022, Revised March 6, 2024, Accepted March 7, 2024*)

Abstract. This article develops a nonclassical size dependent nanoplate model to study the dynamic response of functionally graded carbon nanotube (FGCNT) nanoplates under a moving load. Both nonlocal and microstructure effects are incorporated through the nonlocal strain gradient elasticity theory. To investigate the effect of reinforcement orientation of CNT, four different configurations are studied and analysed. The FGM gradation thorough the thickness direction is simulated using the power law. In the context of the first order shear deformation theory, the dynamic equations of motion and the associated boundary conditions are derived by Hamilton's principle. An analytical solution of the dynamic equations of motion is derived based on the Navier methodology. The proposed model is verified and compared with the available results in the literature and good agreement is found. The numerical results show that the dynamic performance of FGCNT nanoplates could be governed by the reinforcement pattern and volume fraction in addition to the non-classical parameters and the moving load dimensionless parameter. Obtained results are reassuring in design and analysis of nanoplates reinforced with CNTs.
Keywords: analytical solution; dynamic analysis; FGCNT nanoplate; moving point load; nonlocal strain gradient; reinforcement orientation; size dependent

1. Introduction

The functionally graded materials (FGMs) was originated during a space plane project in Japan in 1984, (Alshorbagy *et al*. 2011). FGMs are made from mixture of metals and ceramics with gradation function. The main characteristics of these materials are the smooth and continuous variation of their properties in one or more directions, (She 2021, Tharwan *et al*. 2023). The invention of carbon nanotubes (CNTs) by Iijima (1991) has caused intensive research in science and engineering. Some of the excellent properties of CNTs are high stiffness, low density, very high aspect ratio, remarkable electronic properties, high conductivity and strength. The combination of CNTs as fibre reinforcements into composites and the application of FGMs concept produces a new material called functionally graded carbon nanotube–reinforced composites (FG-CNTRCs). Combining the unique properties of FGMs and superior properties of CNTs, FG-CNTRCs have found broad potential applications in automotive industries, aerospace, ocean and civil engineering, electromechanical equipment, and Nanostructures. A nanoplate is a subclass of nanostructures which have many engineering applications, for instance, in information storage, transducers, solar cells, MEMS/NEMS, and components in nanomachines.

For the first time, the FGM concept was applied by Shen (2009) on CNTRCs. Shen and Zhang (2010) investigated thermal buckling and post buckling behaviour for FG nanocomposite plates reinforced by single-walled carbon nanotubes (SWCNTs) subjected to in-plane temperature variation. Post buckling analysis of FG-CNT reinforced composite cylindrical shell under axial compression and lateral pressure in thermal environments has been performed by Shen (2011). Shen and Zhu (2012) presented compressive post buckling under thermal environments and thermal post buckling due to a uniform temperature rise of a sandwich plate with carbon nanotube-reinforced composite (CNTRC) face sheets resting on an elastic foundation. Lei *et al*. (2013) utilized the Ritz method in order to examine the buckling behaviour of FG CNT strengthened plates employing the first order shear deformation theory (FOSDT) to model the composite plate. Shen and Xiang (2012-2014) examined the nonlinear vibration behaviour of FG-CNT reinforced composite cylindrical shell, panels and beams in thermal environments. Using a meshless approach, Liew *et al*. (2014) present a post buckling analysis of FG-CNT reinforced composite cylindrical panels under axial compression. Rafiee *et al*. (2014) investigated non-linear dynamic stability of piezoelectric FG-CNTRCs plates with initial geometric imperfection and harmonic loading considering various CNTs distributions such as: UD, FG-X, FG-O and FG-V. Employing first-order shear deformation theory (FSDT),

*Corresponding author, Assistant Professor,
E-mail: meltaher@kau.edu.sa; mmeltaher@zu.edu.eg
**Co-corresponding author, Ph.D.,
E-mail: mthaewan@jazanu.edu.sa

ISSN: 2287-237X (Print), 2287-2388 (Online)

they concluded that dynamic instability region for FG-X distribution is greater than other distributions and this region moved to higher frequency with increasing of CNTs volume fraction.

Zhang *et al*. (2015) proposed a state-space method for vibration analysis of FG-CNT composite plates subjected to in-plane loads based on higher-order shear deformation theory. This research analysed three different symmetric linear distributions of the reinforcements along the thickness, namely UD, FG-X and FG-O. They concluded that FG-X provides the largest frequency and critical buckling in-plane load. On the contrary, the frequency for the FGO-CNT plate was the lowest. Zhang and Liew (2015) presented detailed parametric studies of the large deflection behaviours of FG-CNTRC quadrilaterals for different types of CNT distributions. They concluded that the geometric parameters such as side angle, thickness-to-width ratio or plate aspect ratios are more significant than material parameters such as CNT distribution and CNT volume fraction. Phung-Van *et al*. (2015) presented an actual formulation based on higher-order shear deformation theory and isogeometric analysis to obtain the dynamic and static response of FG composite plates. Their numerical findings showed reliability and high accuracy of the suggested approach compared with other available numerical methods. To comprehend the thermal effects, Mirzaei and Kiani (2015, 2016) analysed the buckling behaviour of CNT strengthened plates and conical shells in a thermal environment. Shell and plate structures were modelled using the FOSDT and different types of CNT grading functions. It was shown that type X FG strengthened plates and conical hells have the highest maximum buckling load. Ansari *et al*. (2016) utilized the mapping differential quadrature (DQ) methodology to study the free vibration of carbon nanotube-reinforced composite quadrilateral plates having thermal environments with various classical boundary conditions. Zhang *et al*. (2016) broadened their investigations and performed the first known postbuckling analysis of FG-CNTR plates. They also obtained the bending stiffness through the nodal integration scheme. Specific examinations on the postbuckling response of FG-CNTR plates were conducted to show the effects of plate width-to-thickness ratio, and CNT volume content on the boundaries.

Ghorbanpour *et al*. (2015) analyzed the surface stress effect on the biaxial critical buckling load of nonlocal polymeric nanocomposite rectangular plate reinforced by CNTs. They showed the biaxial critical buckling load decreases with increasing of the CNTs volume fraction. Mohammadimehr *et al*. (2015) performed vibration of viscoelastic piezoelectric polymeric nanocomposite plate reinforced by FG-SWCNTs using meshless method based on modified strain gradient theory (MSGT) and sinusoidal shear deformation theory. They concluded that the natural frequency increases with increasing of elastic foundation parameter, small scale parameters, and magnetic field. Mohammadimehr *et al*. (2016a, b) investigated bending and buckling, and free vibration analysis of micro composite Reddy plate reinforced by FG-SWCNTs embedded in an elastic foundation and hydro-thermal environments with temperature-dependent material properties. The generalized rule of mixture was used to define hydro-thermo-mechanical material properties. Three material length scale parameters were considered by MSGT. Based on the classical plate theory (CPT) and the strain gradient theory (SGT), Mohammadimehr and Mostafavifar (2016) analysed free vibration of sandwich plates with a transversely flexible core and FG-CNTs reinforced nanocomposite face sheets under the influence of magnetic field and temperature-dependent material properties. They considered the influences of aspect and side ratios, temperature changes, core-to-face sheet thickness ratio, distribution types, and volume fraction of CNTs. Mohammadimehr *et al*. (2016b) extended the work in a previous paper (2016a) for biaxial buckling and bending analysis of double-coupled polymeric nanocomposite plates reinforced by functionally graded single-walled boron nitride nanotubes (FG-SWBNNTs) and FG-SWCNTs. The micromechanical approach was utilised to determine the elastic and piezoelectric material properties of the double-coupled nanocomposite rectangular plates. Then, the critical biaxial buckling load and deflection of the double-coupled nanocomposite plates were derived by Navier's method.

Barati (2017) studied forced vibration of nonlocal strain gradient metal foam nanoplates with uniform and graded porosities by using Galerkin's method. Nguyen *et al*. (2017) proposed the isogeometric analysis associated with a novel quasi-3D shear deformation theory to investigate the size-dependent effects within FG microplates. They considered both shear deformations and thickness stretching effect without requiring shear correction factors. Based on the nonlocal theory of Eringen, Phung-Van *et al*. (2017) used isogeometric analysis and generalized higher-order shear deformation theory (HSDT) to investigate the influence of size dependency of FG-CNTRC nanoplates. Four special distributions of carbon nanotubes (CNTs) were considered. Employing the modified couple stress theory, Farzam and Hassani (2018) studied the thermal and mechanical buckling analysis of FG-CNTRC plates using isogeometric analysis and a refined hyperbolic shear deformation theory. Utilising high-order sandwich panel theory and modified strain gradient theory (MSGT), Mohammadimehr *et al*. (2018) investigated free vibration analysis of a micro-magneto-electro-elastic sandwich panel with a transversely flexible core and FG-CNTs reinforced nanocomposite face sheets. Salari *et al*. (2019) studied the impact of porosity-dependent asymmetric on thermal buckling of inhomogeneous annular nonlocal nanoplates resting on elastic substrate. Karami and Karami (2019) develops a four-unknown refined plate theory and the Galerkin method to investigate the size-dependent stability behaviour of FGM under the thermal environment. Kolahdouzan *et al*. (2020) developed a layer-wise theory for reaching precise results of buckling and vibration behaviour of FG-CNTRC annular nanoplates. She *et al*. (2021) studied the resonance analysis of composite curved microbeams reinforced with graphene nanoplatelets. Zhang *et al*. (2021) examined the snap-buckling stability of FGCNTR curved nanobeams considering surface effects. In 2021, Lu *et al*. presented the size-dependent effect on postbuckling response of graphene

reinforced composite microtubes with geometrical imperfection. Alazwari *et al*. (2022) studied the effect of thickness stretching on free vibration, bending and buckling behavior of carbon nanotubes reinforced composite (CNTRC) laminated nanoplates rested on new variable elastic foundation. Daikh *et al*. (2023) developed a three-unknown refined shear beam model for the bending of randomly oriented FG-CNT/fiber-reinforced composite laminated beams rested on a new variable elastic foundation. Drai *et al*. (2023) presented a modified analytical model for the bending behavior of axially functionally graded carbon nanotubes reinforced composite (CNTRC) nanobeams.

Recently, dynamics and stability of structures with moving masses attracted a lot of interests, because of their applications in many civilian and military areas, Assie *et al*. (2021). Bouafia *et al*. (2021) examined the small scale impact on the vibration FG nonlocal elasticity nanoplate embedded in an elastic medium based on the four-unknown refined integral plate theory. Esen *et al*. (2020) and Abdelrahman *et al*. (2021a) studied a vibration response of perforated nonlocal strain gradeint nanobeam under moving load using Navier appraoch. Abdelrahman *et al*. (2021b) and Esen *et al*. (2021a) developed previous model to studied the dynamics of FG nanobeam reinforced by carbon nanotubes and resting on elastic foundation. Eltaher *et al*. (2021) exploited the doublet mechanics theory to analyze the size scale infulance on the mechanical vibration behaviors of nanoscale Timoshenko CNTs under moving load. Esen *et al*. (2021b) studied analytically, the vibration response of symmetric and sigmoid FG Timoshenko nonlocal strain gradeint nanobeam under moving load, and concluded that both resonant frequencies and dynamic time response can be controlled by selecting a suitable FGM distribution. Ding and she (2021) developed a higher-order beam model for the snap-buckling analysis of FG pipes conveying fluid. Xu *et al*. (2021) developed enhanced numerical model to study the response of nanoplate-based mass sensors with corner point supports. Farahmand (2021) studied the buckling of moderately thick microplate using strain gradient theory incorporating two-variable efined plate theory. Liu *et al*. (2021) examined the vibration behavior of laminated nanoplate with piezo-magnetic based on the nonlocal strain gradient theory using the Navier method. Mahesh and Harursampath (2021) investigated nonlinear deflection analysis of CNT/magneto-electro-elastic smart shells under multi-physics loading. Thai *et al*. (2021) presented bending and free vibration analyses a nonlocal strain gradient laminated composites and sandwich nanoplates using meshfree approach.

The current study targets to examine analytically the free and forced vibration behaviors of FGCNTs nonlocal strain gradient nanoplates under moving load, that has not considered before. The different distribution schemes of CNTs through the thickness direction are considered. The size-scale and microstructure-scale have been included in the proposed model. The rest of this paper is organized as following, the constitutive equations, equilibrium equations, and boundary conditions are derived in section 2. Section 3 presented a Navier methodology to solve analytically the equations of motion and find the response equation. Verification of proposed model is presented in section 4. However, sections 5 and 6 presented the numerical results, discussion, and conclusions remarks.

2. Basic equations

2.1 Effective properties of FG-CNT

Consider a composite rectangular microplate having a length *a*, width *b*, thickness *h* under the action of moving load as shown in Fig. 1. Four types of aligned carbon nanotubes (CNT) reinforced plates are considered as shown in Fig. 2, namely uniformly distributed CNT beams (UD-CNT), functionally graded CNT type Λ (FGΛ-CNT) with densified CNT in the lower region, and functionally graded CNT type X (FGX-CNT) with the concentrated CNT in both the upper and lower regions. Functionally graded, TYPE O, (FGO-CNT). The orientations of reinforcing CNT are along the length direction, which is the *x*-axis. It is assumed that all reinforced plates are in the same dimensions with the same total weight m_{TCNT} and volume fraction V_{TCNT} of CNTs, but in the Λ, X and O types, the distribution of the CNTs are according to a power law. Thus, the distribution of the CNTs in FGΛ-CNT in the thickness direction as a function of *z* is given by (Shen 2009, Wattanasakulpong and Ungbhakorn 2013)

$$\mu(z) = \left(\frac{h-2z}{2h}\right)^k, \qquad \left(-\frac{h}{2} \le z \le \frac{h}{2}\right) \tag{1}$$

And the corresponding volume fraction of CNTs is derived as

$$V_{CNT}(z) = (\varphi+1)\left(\frac{h-2z}{2h}\right)^k V_{TCNT}, \qquad \left(-\frac{h}{2} \le z \le \frac{h}{2}\right) \tag{2}$$

where φ refers to the nonlinearity distribution of the CNT shape function, $\varphi \geq 1$. However from the practical perspective, only linear distribution is considered in the current study, i.e. $\varphi = 1$. According to linear distribution, Eq. (2) is rewritten as

$$V_{CNT}(z) = \left(\frac{h-2z}{h}\right)^k V_{TCNT}, \qquad \left(-\frac{h}{2} \le z \le \frac{h}{2}\right) \tag{3}$$

For the considered CNT reinforced distributions, assume that they will have the same geometries and contain the same value of total weight of CNTs m_{TCNT}, and with total CNTs volume fraction V_{TCNT} expressed as, (Abdelrahmaan *et al*. 2022, Zhang *et al*. 2023)

$$V_{TCNT}(z) = \frac{W_{CNT}}{W_{CNT} + \left(\frac{\rho_{CNT}}{\rho_m}\right)\{1 - W_{CNT}\}} \tag{4}$$

and W_{CNT} represents CNT mass volume; ρ_m and ρ_{CNT} denote the matrix and CNT density parameters.

For X type FGX-CNT the distribution and volume fraction of CNTs is (Lin and Xiang 2014)

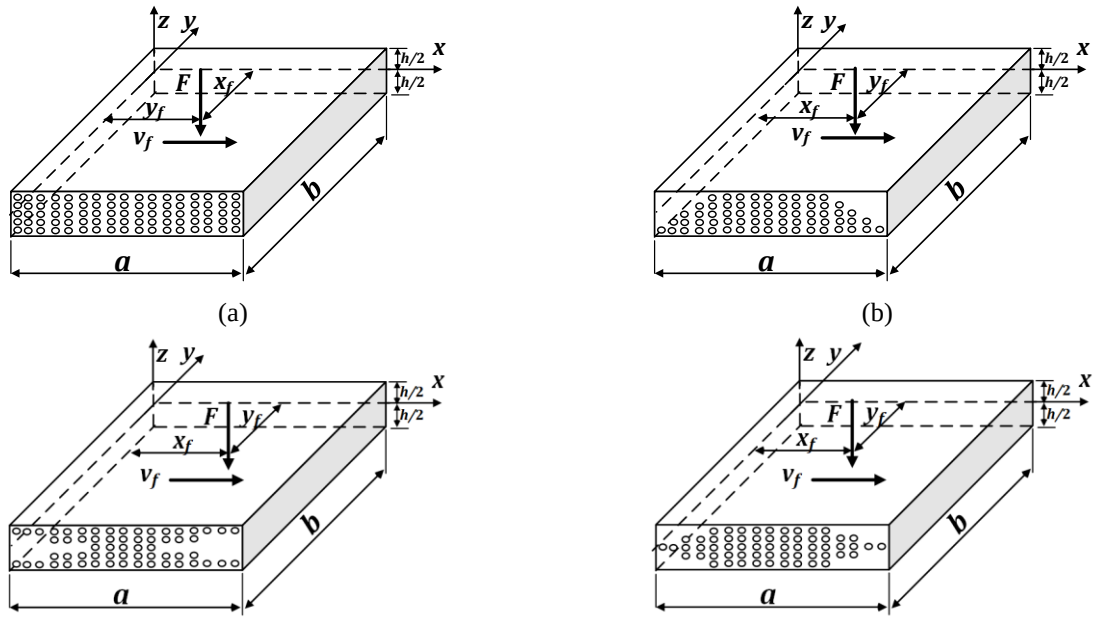

Fig. 1 The carbon nanotube functionally graded plates with different configurations

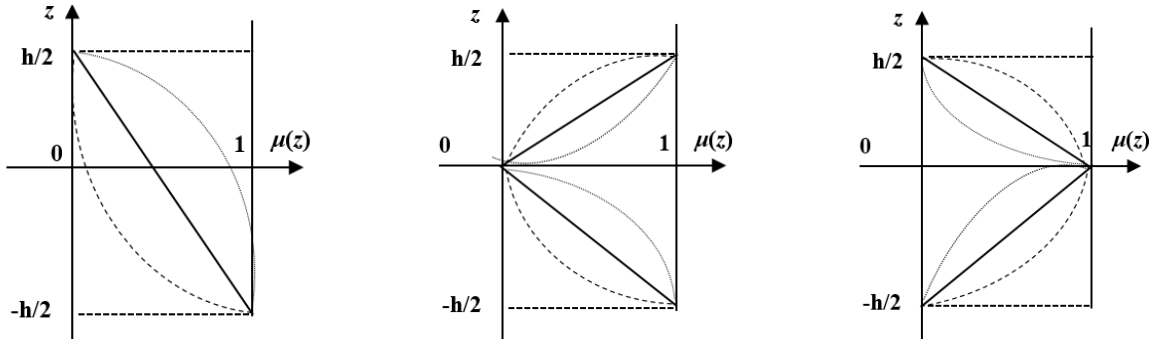

Fig. 2 CNT distribution shape function of FG-CNT plate; (a) Λ-type, (b) X-type, and (c) O-type

$$\mu(z)=\begin{cases}\left(\frac{2z}{h}\right)^k & \left(0\le z\le\frac{h}{2}\right),\\ \left(-\frac{2z}{h}\right)^k & \left(-\frac{h}{2}\le z\le 0\right)\end{cases}$$
$$V_{CNT}(z)=\begin{cases}(k+1)\left(\frac{2z}{h}\right)^k V_{TCNT} & \left(0\le z\le\frac{h}{2}\right),\\ (k+1)\left(-\frac{2z}{h}\right)^k V_{TCNT} & \left(-\frac{h}{2}\le z\le 0\right)\end{cases} \quad (5)$$

For FG-O the distribution and volume fraction (Thang *et al* 2021)

$$\mu(z)=\begin{cases}\left(1-\frac{2z}{h}\right)^k & \left(0\le z\le\frac{h}{2}\right),\\ \left(1+\frac{2z}{h}\right)^k & \left(-\frac{h}{2}\le z\le 0\right)\end{cases} \quad (7)$$

$$V_{CNT}(z)=\begin{cases}(k+1)\left(1-\frac{2z}{h}\right)^k V_{TCNT} & \left(0\le z\le\frac{h}{2}\right),\\ (k+1)\left(1+\frac{2z}{h}\right)^k V_{TCNT} & \left(-\frac{h}{2}\le z\le 0\right)\end{cases} \quad (8)$$

For UD-CNT beams the distribution are uniform along the thickness and the volume fraction of the CNTs is the same as the total volume fraction of the CNTs. Thus,

$$V_{CNT}(z)=V_{TCNT},\quad \left(-\frac{h}{2}\le z\le\frac{h}{2}\right) \quad (9)$$

The shape function distributions for the different functionally graded CNT plate configurations are depicted in Fig. 2.

The effective material properties are evaluated from the results of molecular dynamics simulations (Griebel and Hamaekers 2004, Han and Elliott 2007) and a rule of mixture. The expressions of the properties are (Shen 2009).

$$E_{11}(z)=\eta_1 V_{CNT}(z)E_{11}^{cnt}+V_m(z)E^m, \quad (10a)$$

$$\frac{\eta_2}{E_{22}(z)}=\frac{V_{CNT}(z)}{E_{22}^{cnt}}+\frac{V_m(z)}{E^m}, \quad (10b)$$

$$\frac{\eta_3}{G_{12}(z)}=\frac{V_{CNT}(z)}{G_{12}^{cnt}}+\frac{V_m(z)}{G^m}, \quad (10c)$$

$$\upsilon_{12}(z) = V_{CNT}(z)\upsilon_{12}^{cnt} + V_m(z)\upsilon^m, \tag{10d}$$

$$\upsilon_{21}(z) = \frac{\upsilon_{12}(z)}{E_{11}(z)}E_{22}(z), \tag{10e}$$

$$\rho(z) = V_{CNT}(z)\rho^{cnt} + V_m(z)\rho^m, \tag{10f}$$

$$V_m(z) = 1 - V_{CNT}(z). \tag{10g}$$

Here, E^m, G^m, E_{11}^{cnt}, E_{22}^{cnt}, G_{12}^{cnt} are Young's modulus and shear modulus of matrix and CNT, η_i, (i = 1 , 2 and 3) are efficiency parameters of CNT/matrix; υ^m and υ_{12}^{cnt} are Poisson's ratios of matrix and CNT, and ρ^m and ρ^{cnt} are mass densities of matrix and CNT, respectively.

The effective $E(z)$ and $G(z)$ are given by (Lin and Xiang 2014) as

$$E(z) = \frac{E_{11}(z)}{1 - \upsilon_{12}(z)\upsilon_{21}(z)} \text{ and } G(z) = G_{12}(z) \tag{11}$$

2.2 Nonlocal strain gradient theory (NSGT)

Based on the NSGT, the total stress tensor is expressed as Lim *et al*. (2015):

$$t_{ij} = \sigma_{ij} - \nabla\sigma_{ij,m}^{(1)} \tag{12}$$

where ∇ denotes the Lapacian operator; σ_{ij} and $\sigma_{ij,m}^{(1)}$ are the corresponding stress and the higher order stress tensors which can be expressed as:

$$\begin{Bmatrix} \sigma_{ij} \\ \sigma_{ijm}^{(1)} \end{Bmatrix} = \begin{Bmatrix} \int_V \alpha_0(\boldsymbol{x}', \boldsymbol{x}, e_0 a) C_{ijkl}\varepsilon'_{kl} dV' \\ l^2 \int_V \alpha_1(\boldsymbol{x}', \boldsymbol{x}, e_1 a) C_{ijkl}\varepsilon'_{kl,m} dV' \end{Bmatrix} \tag{13}$$

where e_0 a and e_1 a are known as two nonlocal parameters, l is also a characteristic length that has been introduced in Eq. (13) to account for the strain gradient elasticity effect. Herein, $\alpha_0(\boldsymbol{x}', \boldsymbol{x}, e_0 a)$ and $\alpha_1(\boldsymbol{x}', \boldsymbol{x}, e_1 a)$ represent two kernel parameters.

Considering $e_0 = e_1 = e$ and (α_0, α_1) satisfy the corresponding condition reported in Eringen, (1983), the stress-strain relations have been introduced in (13) can be given by, (Thang *et al.* 2021)

$$(1 - (ea)^2\nabla^2)\begin{Bmatrix} \sigma_{ij} \\ \sigma_{ijm}^{(1)} \end{Bmatrix} = \begin{Bmatrix} C_{ijkl}\,\varepsilon_{kl} \\ l^2 C_{ijkl}\,\varepsilon_{kl,m} \end{Bmatrix} \tag{14}$$

According to Eq. (12), the total stress tensor can be cast in the following form:

$$(1 - (ea)^2\nabla^2)t_{ij} = (1 - l^2\nabla^2)C_{ijkl}\varepsilon_{kl} \tag{15}$$

2.3 Kinematic equations

Based on the 1st order shear deformation theory (FSDT), the displacement field functions ($u(x, y, z, t)$, $v(x, y, z, t)$, $w(x, y, z, t)$) are given by, (Reddy 2003, Thang *et al.* 2021).

$$\begin{aligned} u(x, y, z, t) &= u_0(x, y, t) + z\phi_x(x, y, t), \\ v(x, y, z, t) &= v_0(x, y, t) + z\phi_y(x, y, t), \end{aligned} \tag{16}$$

$$w(x, y, z, t) = w_0(x, y, t)$$

Here, u, v and w denote the displacement field functions and $u_0(x, y, t)$ $v_0(x, y, t)$ and $w(x, y, t)$ represent the mid-plane displacements in x, y and z axes respectively, and $\phi_x(x, y, t)$ and $\phi_y(x, y, t)$ are the rotation of the cross-section . Thus, the strain components are expressed as, Reddy (2003):

$$\begin{aligned} \varepsilon_{xx} &= \varepsilon_{xx}^0 + z\kappa_x = \frac{\partial u_0}{\partial x} + z\,\frac{\partial \phi_x}{\partial x}, \\ \varepsilon_{yy} &= \varepsilon_{yy}^0 + z\kappa_y = \frac{\partial v_0}{\partial y} + z\,\frac{\partial \phi_y}{\partial y}, \\ \gamma_{yz} &= \gamma_{yz}^0 = \frac{\partial w_0}{\partial y} + \phi_y \\ \gamma_{xz} &= \gamma_{xz}^0 = \frac{\partial w_0}{\partial x} + \phi_x \\ \gamma_{xy} &= \gamma_{xy}^0 + z\kappa_{xy} = \frac{\partial u_0}{\partial y} + \frac{\partial v_0}{\partial x} + z\left(\frac{\partial \phi_x}{\partial y} + \frac{\partial \phi_y}{\partial x}\right) \end{aligned} \tag{17}$$

Incorporating the nonlocal strain gradient effect, the constitutive relationships can be expressed as follows, (Thang *et al.* 2021):

$$\begin{aligned} &(1 - (ea)^2\nabla^2)\begin{Bmatrix} \sigma_{xx} \\ \sigma_{yy} \\ \tau_{yz} \\ \tau_{xz} \\ \tau_{xy} \end{Bmatrix} \\ &= (1 - l^2\nabla^2)\begin{Bmatrix} \left(\frac{E_{11}(z)}{1 - \nu_{12}(z)\nu_{21}(z)}\right)(\varepsilon_{xx} + \nu_{21}(z)\varepsilon_{yy}) \\ \left(\frac{E_{22}(z)}{1 - \nu_{12}(z)\nu_{21}(z)}\right)(\nu_{12}(z)\varepsilon_{xx} + \varepsilon_{yy}) \\ G_{23}(z)\gamma_{yz} \\ G_{13}(z)\gamma_{xz} \\ G_{12}(z)\gamma_{xy} \end{Bmatrix} \end{aligned} \tag{18}$$

Eq. (18) can be rewritten in the following matrix form:

$$\begin{aligned} &(1 - (ea)^2\nabla^2)\begin{Bmatrix} \sigma_{xx} \\ \sigma_{yy} \\ \tau_{yz} \\ \tau_{xz} \\ \tau_{xy} \end{Bmatrix} = (1 - l^2\nabla^2) \\ &\begin{bmatrix} Q_{11}(z) & Q_{12}(z) & 0 & 0 & 0 \\ Q_{12}(z) & Q_{22}(z) & 0 & 0 & 0 \\ 0 & 0 & Q_{44}(z) & 0 & 0 \\ 0 & 0 & 0 & Q_{55}(z) & 0 \\ 0 & 0 & 0 & 0 & Q_{66}(z) \end{bmatrix}\begin{Bmatrix} \varepsilon_{xx} \\ \varepsilon_{yy} \\ \gamma_{yz} \\ \gamma_{xz} \\ \gamma_{xy} \end{Bmatrix} \end{aligned} \tag{19}$$

In which the stiffness constants are expressed as

$$\begin{aligned} &Q_{11} = \frac{E_{11}(z)}{1 - \upsilon_{12}(z)\upsilon_{21}(z)}, \quad Q_{12} = \frac{\upsilon_{12}(z)\,E_{22}(z)}{1 - \upsilon_{12}(z)\upsilon_{21}(z)} \\ &Q_{22} = \frac{E_{22}(z)}{1 - \upsilon_{12}(z)\upsilon_{21}(z)}, \qquad Q_{44} = G_{23}(z), \\ &Q_{55} = G_{13}(z), \qquad Q_{66} = G_{12}(z) \end{aligned} \tag{20}$$

The normal, shear forces, N_{xx}, N_{yy} and N_{xy} bending moments, M_{xx}, M_{yy} and M_{xy} and transverse shear forces, Q_{xx} and Q_{yy} are expressed as.

$$\begin{Bmatrix} N_{xx} \\ N_{yy} \\ N_{xy} \end{Bmatrix} = \int_{-\frac{h}{2}}^{\frac{h}{2}} \begin{Bmatrix} \sigma_{xx} \\ \sigma_{yy} \\ \tau_{xy} \end{Bmatrix} dz, \quad \begin{Bmatrix} M_{xx} \\ M_{yy} \\ M_{xy} \end{Bmatrix} = \int_{-\frac{h}{2}}^{\frac{h}{2}} \begin{Bmatrix} \sigma_{xx} \\ \sigma_{yy} \\ \tau_{xy} \end{Bmatrix} z dz, \tag{21}$$

and $\begin{Bmatrix} Q_{xx} \\ Q_{yy} \end{Bmatrix} = \int_{-h/2}^{h/2} \begin{Bmatrix} \tau_{xz} \\ \tau_{yz} \end{Bmatrix} dz$

2.4 Variational formulation

Applying the Hamiltonian principle, the system of equations of motion can be expressed as follows, Reddy (2007):

$$0 = \int_{t_1}^{t_2} (\delta K - \delta U + \delta V)\, dt \tag{22}$$

where δU presents the variation of the deformation energy

$$\delta U = \frac{1}{2}\int_V \delta(\sigma_{xx}\varepsilon_{xx} + \sigma_{yy}\varepsilon_{yy} + \tau_{xy}\gamma_{xy} + \tau_{xz}\gamma_{xz} + \tau_{yz}\gamma_{yz})dV \tag{23}$$

Using Eqs. (17) and (21), Eq. (23) can be rewritten as

$$\begin{aligned}\delta U = \int_V \big(&N_{xx}\delta u_{0,x} + N_{yy}\delta v_{0,x} + N_{xy}\big(\delta u_{0,x} + \delta v_{0,x}\big) \\ &+ M_{xx}\,\delta\phi_{x,x} + M_{yy}\delta\phi_{y,y} + M_{xy}(\,\delta\phi_{x,y} \\ &+ \delta\phi_{y,x}) + Q_{xx}(\delta w_{0,x} + \delta\phi_x) \\ &+ Q_{yy}(\delta w_{0,y} + \delta\phi_y)\big)dV\end{aligned} \tag{24}$$

δT refers to the variation of the kinetic energy

$$\delta T = \frac{1}{2}\int_0^a \int_0^b \int_{-h/2}^{h/2} \delta\{\rho(z)[(\dot{u}^2 + \dot{v}^2 + \dot{w}^2)]\}\, dzdydx \tag{25}$$

Eq. (25) can be rewritten as

$$\begin{aligned}\delta T &= \int_0^a \int_0^b \int_{-\frac{h}{2}}^{\frac{h}{2}} \rho(z) \begin{bmatrix} \big(\dot{u}_0 + z\dot{\phi}_x\big)\big(\delta\dot{u}_0 + z\delta\dot{\phi}_x\big) + \\ \big(\dot{v}_0 + z\dot{\phi}_y\big)\big(\delta\dot{v}_0 + z\delta\dot{\phi}_y\big)\dot{v}^2 \\ +\dot{w}_0\delta\dot{w}_0) \end{bmatrix} dzdydx \\ &= \int_0^a \int_0^b \begin{matrix} I_0(\dot{u}_0\delta\dot{u}_0 + \dot{v}_0\delta\dot{v}_0 + \dot{w}_0\delta\dot{w}_0) \\ +I_1\big(\dot{\phi}_x\delta\dot{u}_0 + \dot{u}_0\delta\dot{\phi}_x + \dot{v}_0\delta\dot{\phi}_y + \dot{\phi}_y\delta\dot{v}_0\big) \\ +I_2(\dot{\phi}_x\delta\dot{\phi}_x + \dot{\phi}_y\delta\dot{\phi}_y)dydx \end{matrix}\end{aligned} \tag{26}$$

The variation of external potential energy,

$$\delta V = \int_V [q(x,y,t)\delta w_0]\, dV \tag{27}$$

where q (*x*,*y*, *t*) is the transverse load.

Evaluating integrals in Eqs (24), (26) and (27) and substitute in the Hamilton principle given in Eq. (22) and setting each coefficient of δu_0, δv_0, δw_0, $\delta\phi_x$ and $\delta\phi_y$ to zero, the set of equations of motion are given by:

$$\begin{aligned}&\delta u_0: \frac{\partial N_{xx}}{\partial x} + \frac{\partial N_{xy}}{\partial y} = I_0\frac{\partial^2 u_0}{\partial t^2} + I_1\frac{\partial^2\phi_x}{\partial t^2}, \\ &\delta v_0: \frac{\partial N_{xy}}{\partial x} + \frac{\partial N_{yy}}{\partial y} = I_0\frac{\partial^2 v_0}{\partial t^2} + I_1\frac{\partial^2\phi_y}{\partial t^2}, \\ &\delta w_0: \frac{\partial Q_{xx}}{\partial x} + \frac{\partial Q_{yy}}{\partial y} + q = I_0\frac{\partial^2 w_0}{\partial t^2}, \\ &\delta\phi_x: \frac{\partial M_{xx}}{\partial x} + \frac{\partial M_{xy}}{\partial y} - Q_{xx} = I_1\frac{\partial^2 u_0}{\partial t^2} + I_2\frac{\partial^2\phi_x}{\partial t^2}, \\ &\delta\phi_x: \frac{\partial M_{xy}}{\partial x} + \frac{\partial M_{yy}}{\partial y} - Q_{yy} = I_1\frac{\partial^2 v_0}{\partial t^2} + I_2\frac{\partial^2\phi_y}{\partial t^2}\end{aligned} \tag{28}$$

With the inertia coefficients:

$$(I_0, I_1, I_2) = \int_{-h/2}^{h/2} \rho(z)(1, z, z^2)dz \tag{29}$$

By substituting (NSGT), (14, 15 16) into (23)

$$\begin{aligned}&\left(1 - l_m^2\frac{\partial^2}{\partial x^2}\right)\begin{pmatrix} A_{11}\dfrac{\partial^2 u_0}{\partial x^2} + A_{12}\dfrac{\partial^2 v_0}{\partial x\partial y} \\ +A_{66}\left(\dfrac{\partial^2 v_0}{\partial x\partial y} + \dfrac{\partial^2 u_0}{\partial y^2}\right) + B_{11}\dfrac{\partial^2\phi_x}{\partial x^2} \\ +B_{12}\dfrac{\partial^2\phi_y}{\partial x\partial y} + B_{66}\left(\dfrac{\partial^2\phi_y}{\partial x\partial y} + \dfrac{\partial^2\phi_x}{\partial y^2}\right)\end{pmatrix} \\ &+\left(1 - (ea)^2\frac{\partial^2}{\partial x^2}\right)\left(-I_0\frac{\partial^2 u_0}{\partial t^2} - I_1\frac{\partial^2\phi_x}{\partial t^2}\right) = 0.\end{aligned} \tag{30a}$$

$$\begin{aligned}&\left(1 - l_m^2\frac{\partial^2}{\partial x^2}\right)\begin{pmatrix} A_{12}\dfrac{\partial^2 u_0}{\partial x\partial y} + A_{22}\dfrac{\partial^2 v_0}{\partial y^2} \\ +A_{66}\left(\dfrac{\partial^2 u_0}{\partial x\partial y} + \dfrac{\partial^2 v_0}{\partial x^2}\right) + B_{22}\dfrac{\partial^2\phi_y}{\partial y^2} \\ +B_{12}\dfrac{\partial^2\phi_x}{\partial x\partial y} + B_{66}\left(\dfrac{\partial^2\phi_x}{\partial x\partial y} + \dfrac{\partial^2\phi_y}{\partial x^2}\right)\end{pmatrix} \\ &+\left(1 - (ea)^2\frac{\partial^2}{\partial x^2}\right)\left(-I_0\frac{\partial^2 v_0}{\partial t^2} - I_1\frac{\partial^2\phi_y}{\partial t^2}\right) = 0.\end{aligned} \tag{30b}$$

$$\begin{aligned}&\left(1 - l_m^2\frac{\partial^2}{\partial x^2}\right)\begin{pmatrix} k_s A_{55}\left(\dfrac{\partial^2 w_0}{\partial x^2} + \dfrac{\partial\phi_x}{\partial x}\right) \\ +k_s A_{44}\left(\dfrac{\partial^2 w_0}{\partial y^2} + \dfrac{\partial\phi_y}{\partial y}\right)\end{pmatrix} \\ &+\left(1 - (ea)^2\frac{\partial^2}{\partial x^2}\right)\left(-q - I_0\frac{\partial^2 w_0}{\partial t^2}\right) = 0.\end{aligned} \tag{30c}$$

$$\begin{aligned}&\left(1 - l_m^2\frac{\partial^2}{\partial x^2}\right) \\ &\begin{pmatrix} B_{11}\dfrac{\partial^2 u_0}{\partial x^2} + B_{12}\dfrac{\partial^2 v_0}{\partial x\partial y} + D_{11}\dfrac{\partial^2\phi_x}{\partial x^2} \\ +D_{12}\dfrac{\partial^2\phi_y}{\partial x\partial y} + B_{66}\left(\dfrac{\partial^2 v_0}{\partial x\partial y} + \dfrac{\partial^2 u_0}{\partial y^2}\right) \\ +D_{66}\left(\dfrac{\partial^2\phi_y}{\partial x\partial y} + \dfrac{\partial^2\phi_x}{\partial y^2}\right) - k_s A_{55}\left(\dfrac{\partial w_0}{\partial x} + \phi_x\right)\end{pmatrix} \\ &+\left(1 - (ea)^2\frac{\partial^2}{\partial x^2}\right)\left(-I_1\frac{\partial^2 u_0}{\partial t^2} - I_2\frac{\partial^2\phi_x}{\partial t^2}\right) = 0\end{aligned} \tag{30d}$$

$$\begin{aligned}&\left(1 - l_m^2\frac{\partial^2}{\partial x^2}\right) \\ &\begin{pmatrix} B_{22}\dfrac{\partial^2 v_0}{\partial y^2} + B_{12}\dfrac{\partial^2 u_0}{\partial x\partial y} + D_{22}\dfrac{\partial^2\phi_y}{\partial y^2} \\ +D_{12}\dfrac{\partial^2\phi_x}{\partial x\partial y} + B_{66}\left(\dfrac{\partial^2 u_0}{\partial x\partial y} + \dfrac{\partial^2 v_0}{\partial x^2}\right) \\ +D_{66}\left(\dfrac{\partial^2\phi_x}{\partial x\partial y} + \dfrac{\partial^2\phi_y}{\partial x^2}\right) - k_s A_{44}\left(\dfrac{\partial w_0}{\partial y} + \phi_y\right)\end{pmatrix} \\ &+\left(1 - (ea)^2\frac{\partial^2}{\partial x^2}\right)\left(-I_1\frac{\partial^2 v_0}{\partial t^2} - I_2\frac{\partial^2\phi_y}{\partial t^2}\right) = 0.\end{aligned} \tag{30e}$$

$$\begin{aligned}(A_{11}, B_{11}, D_{11}) = \textstyle\int_{-h/2}^{h/2}(1, z, z^2)Q_{11}dz \quad \text{and} \\ (A_{12}, B_{12}, D_{12}) = \textstyle\int_{-h/2}^{h/2}(1, z, z^2)Q_{12}dz\end{aligned} \tag{31a}$$

$$(A_{22}, B_{22}, D_{22}) = \int_{-\frac{h}{2}}^{\frac{h}{2}}(1, z, z^2)Q_{22}dz \tag{31b}$$

$$\text{and } (A_{66}, B_{66}, D_{66}) = \int_{-h/2}^{h/2} (1, z, z^2) Q_{66} dz$$

$$A_{44} = \int_{-h/2}^{h/2} Q_{44} dz \quad \text{and} \quad A_{55} = \int_{-h/2}^{h/2} Q_{55} dz \tag{31c}$$

For FGM the transverse shear correction factor k_s is given by (Zhu *et al*. 2012a):

$$k_s = \frac{5}{6 - (\upsilon^m \mathrm{V}^m + \upsilon_{12}^{cnt} V_{TCNT})} \tag{32}$$

3. Analytical solution

For the current analysis, we proposed all problems with simply supported boundary conditions. For the classical boundary conditions in (at $x, y = 0$ and $x, y = a, b$)

$$\begin{aligned} N_{xx} &= 0, \quad N_{yy} = 0, \quad N_{xy} = 0, \quad w = 0, \\ M_{xx} &= 0, \quad M_{yy} = 0, \quad M_{xy} = 0, \end{aligned} \tag{33}$$

And for non-classical boundary conditions (at $x, y = 0$ and $x, y = a, b$)

$$\begin{aligned} &\frac{\partial u_0}{\partial x} = 0, \quad \frac{\partial v_0}{\partial x} = 0, Q_{xx}^h = 0, \quad Q_{yy}^h = 0, \\ &\frac{\partial \phi_x}{\partial x} = 0, \quad \frac{\partial \phi_y}{\partial y} = 0 \end{aligned} \tag{34}$$

Therefore, the Navier's approach will be used to define the vibration frequencies and displacements. Assuming the vibration solution is periodic in time, the displacements are in the form:

$$w_0(x,t) = \sum_m \sum_n W_{mn} \sin(\alpha x) \sin(\beta y)\, e^{i\omega_{mn} t} \tag{35a}$$
$$\alpha = \left(\frac{m\pi}{a}\right), \beta = \left(\frac{n\pi}{b}\right), \; i = \sqrt{-1}$$

$$u_0(x,t) = \sum_m \sum_n U_{mn} \cos(\alpha x) \sin(\beta y)\, e^{i\omega_{mn} t}. \tag{35b}$$

$$v_0(x,t) = \sum_m \sum_n V_{mn} \sin(\alpha x) \cos(\beta y)\, e^{i\omega_{mn} t}. \tag{35c}$$

$$\phi_x(x,t) = \sum_m \sum_n \mathrm{X}_{mn} \cos(\alpha x) \sin(\beta y)\, e^{i\omega_{mn} t} \tag{35d}$$

$$\phi_y(x,t) = \sum_m \sum_n \mathrm{Y}_{mn} \sin(\alpha x) \cos(\beta y)\, e^{i\omega_{mn} t} \tag{35e}$$

where ω_{mn} is the natural vibration frequencies. For any U_{mn}, V_{mn} W_{mn}, X_{mn} and Y_{mn} the series solution (35) satisfies the classical and non-classical boundary conditions in (33) and (34). Substituting Eqs. (35) into Eqs. (30) the following Eigen value equation is derived.

$$(\mathbf{K} - \omega_{mn}^2 \mathbf{M})\mathbf{d} = 0 \tag{36}$$

Here, $\mathbf{d} = \{U_{mn} \quad V_{mn} \quad W_{mn} \quad X_{mn} \quad Y_{mn}\}^{\boldsymbol{T}}$ are the unknowns to be determined, and $\mathbf{M}$ are stiffness and mass matrices, respectively. And the coefficients of them are described as follows:

$$\begin{gathered} \mathbf{K}_{11} = (A11\alpha^2 + A66\beta^2)c_2, \\ \mathbf{K}_{12} = (A12 + A66)\beta\alpha c_2, \quad \mathbf{K}_{13} = \mathbf{0}, \\ \mathbf{K}_{14} = (B11\alpha^2 + B66\beta^2)c_2, \\ \mathbf{K}_{15} = (B12 + B66)\beta\alpha, \mathbf{K}_{21} = \mathbf{K}_{12}, \\ \mathbf{K}_{22} = (A66\alpha^2 + A22\beta^2)c_2, \quad \mathbf{K}_{23} = \mathbf{0}, \\ \mathbf{K}_{24} = \mathbf{K}_{15}, \; \mathbf{K}_{25} = (B66\alpha^2 + B22\beta^2)c_2, \\ \mathbf{K}_{31} = \mathbf{K}_{32} = 0, \; \mathbf{K}_{33} = (k_s A_{55}\alpha^2 + k_s A_{44}\beta^2)c_2, \\ \mathbf{K}_{34} = -k_s A_{55}\alpha c_2, \; \mathbf{K}_{35} = k_s A_{44}\beta c_2, \; \mathbf{K}_{41} = \mathbf{K}_{14}, \\ \mathbf{K}_{42} = \mathbf{K}_{15}, \; \mathbf{K}_{43} = k_s A_{55}\alpha c_2, \\ \mathbf{K}_{44} = (D11\alpha^2 + D66\beta^2 + k_s A_{55})c_2, \\ \mathbf{K}_{45} = (D12 + D66)\beta\alpha c_2, \; \mathbf{K}_{51} = \mathbf{K}_{42}, \\ \mathbf{K}_{52} = \mathbf{K}_{25}, \; \mathbf{K}_{53} = \mathbf{K}_{35}, \; \mathbf{K}_{54} = (D22 + D66)\beta\alpha c_2, \\ \mathbf{K}_{55} = (D66\alpha^2 + D22\beta^2 + k_s A_{44})c_2, \\ \mathbf{M}_{11} = I_0 c_1, \; \mathbf{M}_{12} = 0, \mathbf{M}_{13} = 0, \mathbf{M}_{14} = I_1 c_1, \\ \mathbf{M}_{15} = 0, \; \mathbf{M}_{21} = 0, \; \mathbf{M}_{22} = I_0 c_1, \; \mathbf{M}_{23} = 0, \\ \mathbf{M}_{24} = 0, \; \mathbf{M}_{25} = I_1 c_1, \; \mathbf{M}_{31} = \mathbf{0}, \; \mathbf{M}_{32} = \mathbf{0}, \\ \mathbf{M}_{33} = I_0 c_1, \; \mathbf{M}_{34} = 0, \; \mathbf{M}_{35} = 0, \; \mathbf{M}_{41} = \mathbf{M}_{25}, \\ \mathbf{M}_{42} = \mathbf{M}_{43} = 0, \; \mathbf{M}_{44} = I_2 c_1, \; \mathbf{M}_{45} = 0 \\ \mathbf{M}_{51} = 0, \; \mathbf{M}_{52} = I_1 c_1, \; \mathbf{M}_{53} = 0, \; \mathbf{M}_{54} = 0, \\ \mathbf{M}_{55} = I_2 c_1, \; c_1 = 1 + (ea)^2\beta^2, \; c_2 = 1 + l_m^2\beta^2 \end{gathered} \tag{37}$$

For the forced vibration response of the FG nano plate, substituting Eqs. (35) into (30) one can derive the following equation:

$$\mathbf{M}\ddot{\mathbf{d}} + \mathbf{K}\,\mathbf{d} = \mathbf{F} \tag{38}$$

where $\mathbf{F}$ is the external force vector and it can be defined according to the type of the transverse load $q(x)$ as given below (Reddy 2007):

$$\mathbf{F} = \begin{Bmatrix} 0 \\ 0 \\ Q_{mn} c_1 \\ 0 \\ 0 \end{Bmatrix} \tag{39}$$

The external load can be expanded in Fourier series and the term Q_{mn} is defined as follows:

$$q(x) = \textstyle\sum_m \sum_n Q_{mn} \sin(\alpha x) \sin(\beta y) \tag{40a}$$

$$Q_{mn} = \tfrac{4}{ab} \textstyle\int_0^a \int_0^b q(x) \sin(\alpha x) \sin(\beta y)\, dxdy \tag{40b}$$

For point load at (x_p, y_p), the external load is defined as $q(x, y, t) = F\delta(x - x_p, y - y_p)$ and Q_{mn} is derived as:

$$\begin{aligned} Q_{mn} &= \frac{4F}{ab} \int_0^a \int_0^b \sin\left(\frac{m\pi}{a}(x_p \right. \\ &\qquad \left. = vt)\right) \sin\left(\frac{n\pi}{b} y_p\right) dxdy, \\ &m, n = 1, 3, 5, \ldots \\ x_p, y_p &= a, \frac{b}{2}; \xrightarrow{yields} Q_{mn} = \frac{4F}{ab} \sin\frac{m\pi}{2} \sin\frac{n\pi}{2}, \\ &m, n = 1, 3, 5, \ldots \end{aligned} \tag{41}$$

For uniform load (Tran *et al* 2020):

$$q(x) = q_0, \qquad Q_{mn} = \frac{16 q_0}{mn\pi^2}, \qquad m, n = 1, 3, 5, \ldots \tag{42}$$

Table 1 CNT efficiency parameters (Lin and Xiang 2014)

CNT efficiency parameters	V_{TCNT}		
	0.12	0.17	0.28
η_1	0.137	0.142	0.141
η_2	1.022	1.626	1.585
η_3	0.715	1.138	1.109

Table 2 Comparison of non-dimensional frequencies $\lambda = \omega_i a^2\sqrt{\rho_m/(E_m h^2)}$ for the effects of width-to-thickness ratio and CNT volume fraction, SSSS square UD and FGΛ plates

V_{TCNT}	b/h	Modes (m,n)	UD				FGΛ			
			Present	ANSYS	(Zhu *et al*. 2012a)	Thang 2021	Present	ANSYS	(Zhu *et al*. 2012a)	Thang 2021
0.17	10	(1,1)	14.9412	14.9501	16.815	15.3333	13.7671	13.7675	15.461	14.1528
		(1,2)	22.0125	22.0121	22.063	-	21.4908	21.4901	21.307	-
		(1,3)	24.3326	24.3325	24.337	-	24.4857	24.4853	24.511	-
		(1,4)	24.3348	24.3345	24.337	-	24.4851	24.4854	24.511	-
		(2,1)	34.1414	34.1415	34.448	-	34.4942	34.4942	34.273	-
		(2,2)	40.5359	40.5356	40.630	-	39.2374	39.2371	39.263	-
	20	(1,1)	21.4227	21.4223	21.456	-	18.6285	18.6283	18.638	-
		(1,2)	26.6158	26.6155	26.706	-	24.6996	24.6995	24.734	-
		(1,3)	39.9779	39.9774	40.401	-	39.0483	39.0484	39.471	-
		(1,4)	48.6695	48.6694	48.674	-	48.9724	48.9723	49.023	-
		(2,1)	48.6695	48.6694	48.674	-	48.9723	48.9721	49.023	-
		(2,2)	61.3728	61.3725	62.723	-	58.8556	58.8552	59.191	-

Table 3 Comparison of non-dimensional frequencies $\lambda = \omega_i a^2\sqrt{\rho_m/(E_m h^2)}$ for the effects of width-to-thickness ratio and CNT volume fraction, SSSS square FGO and FGX plates

V_{TCNT}	b/h	Modes (m,n)	FGO				FGX			
			Present	ANSYS	(Zhu *et al*. 2012a)	Thang 2021	Present	ANSYS	(Zhu *et al*. 2012a)	Thang 2021
0.17	10	(1,1)	12.7985	12.7988	14.282	13.0976	16.2192	16.2193	18.278	16.6524
		(1,2)	20.2693	20.2694	20.091	-	23.7606	23.7605	23.541	-
		(1,3)	24.4862	24.4864	24.512	-	24.4866	24.4845	24.512	-
		(1,4)	24.4865	24.4867	24.512	-	24.4863	24.4867	24.512	-
		(2,1)	32.9834	32.9831	32.766	-	36.5119	36.5126	36.245	-
		(2,2)	37.7551	37.7553	37.763	-	42.1311	42.1319	42.150	-
	20	(1,1)	16.6402	16.6403	16.628	-	24.7352	24.7345	24.764	-
		(1,2)	22.7103	22.7105	22.739	-	29.8093	29.8029	29.819	-
		(1,3)	36.7195	36.7194	37.139	-	43.2574	43.2565	43.612	-
		(1,4)	48.9726	48.9723	49.024	-	48.9728	48.9735	49.024	-
		(2,1)	48.9724	48.9724	49.024	-	48.9724	48.9735	49.024	-
		(2,2)	54.0993	54.0998	54.367	-	65.0743	65.0737	66.616	-

4. Verification of the solution methodology

To check and verify the accuracy of the proposed solution methodology, consider a SSSS square nanoplate with the following material properties (Lin and Xiang 2014, Shen amd Xiang 2012): $E^m = 2.5\,GPa$, $\upsilon^m = 0.3$, $E_{11}^{cnt} = 5646.6\,GPa$, $E_{22}^{cnt} = 7080\,GPa$, $G_{12}^{cnt} = 1944.5\,Gpa$, $\upsilon_{12}^{cnt} = 0.175$, $\rho^m = 1190\,kg/m^3$, $\rho^{cnt} = 2100\ kg/m^3$, $h = 0.1\,m$, with the efficiency parameters of CNT in Table 1 (Lin and Xiang 2014).

For comparison of the present formulation some numerical simulations have been carried out using ANSYS and present formulation for SSSS boundary conditions are considered. Tables 2 and 3 show the comparisons of the fundamental non-dimensional frequency parameters for total CNT volume fraction $V_{TCNT} = 0.17$ and UD, FGΛ, FGX and FGO nanoplates. The result are in a good agreement with the literature studies especially with the

Table 4 Comparisons of dimensionless frequencies $\lambda_{mn} = \omega_{mn} a^2 \sqrt{\rho_m/(E_m h^2)}$ of UD-CNT nanoplates for V_{TCNT} and $e_0 a$ and $l_m\ (nm), b/a = 1, a/h = 10, and\ m = 1, n = 1$. SSSS

	$V_{TCNT} = 0.12$			$V_{TCNT} = 0.17$			$V_{TCNT} = 0.28$		
$e_0 a$	$l_m = 0$	$l_m = 1$	$l_m = 2$	$l_m = 0$	$l_m = 1$	$l_m = 2$	$l_m = 0$	$l_m = 1$	$l_m = 2$
0	12.038725	13.151692	16.159082	14.941245	16.322550	20.055025	16.337574	17.847961	21.929247
0.5	11.892899	12.992385	15.963345	14.760261	16.124832	19.812096	16.139675	17.631763	21.663614
1	11.019946	12.038728	14.791618	13.676843	14.941248	18.357862	14.955005	16.337574	20.073477
1.5	10.048860	10.977864	13.488170	12.471627	13.624619	16.740156	13.637161	14.897894	18.304588
2	8.9690037	9.7981768	12.038727	11.131421	12.160510	14.941252	12.171704	13.296961	16.337570

Table 5 Comparisons of dimensionless frequencies $\lambda_{mn} = \omega_{mn} a^2 \sqrt{\rho_m/(E_m h^2)}$ of FGΛ -CNT nanoplates for V_{TCNT} and $e_0 a$ and $l_m\ (nm), b/a = 1, a/h = 10, and\ m = 1, n = 1$. SSSS

	$V_{TCNT} = 0.12$			$V_{TCNT} = 0.17$			$V_{TCNT} = 0.28$		
$e_0 a$	$l_m = 0$	$l_m = 1$	$l_m = 2$	$l_m = 0$	$l_m = 1$	$l_m = 2$	$l_m = 0$	$l_m = 1$	$l_m = 2$
0	11.302929	12.347873	15.171464	13.767149	15.039896	18.479067	15.656172	17.103569	21.014652
0.5	11.166015	12.198301	14.987687	13.600382	14.857713	18.255234	15.466522	16.896387	20.760096
1	10.346417	11.302934	13.887574	12.602102	13.767139	16.915272	14.331265	15.656172	19.236275
1.5	9.4346838	10.306908	12.663793	11.491595	12.553971	15.424686	13.068387	14.276535	17.541162
2	8.4208269	9.1993237	11.302934	10.256703	11.204915	13.767140	11.664052	12.742375	15.656182

results of (Zhu *et al*. 2012b) and the results of commercial software ANSYS.

5. Results and discussions

To demonstrate the capability of the proposed procedure to study and analyze the dynamic behavior of functionally graded CNT nanoplates with different configurations, consider a SSSS square nanoplate with the following geometrical characteristics: a=b=100×10^{-9} m, a/h=10 h. the material characteristics reported in section 4 are used for the considered nanoplates. The developed methodology is applied to detect the free and forced vibration behaviour of the functionally graded composite nanoplate under the action of moving load.

5.1 Free vibration behaviour

Variations of the non-dimensional frequency parameters, λ_{11} with the nonlocality and material size parameters at different values of volume fractions, V_{TCNT} for different CNT configurations are shown in Tables 4-7.

It is noticed that, keeping constant value for the material size parameter, increasing the nonlocality parameter increases the material flexibility and decreases the non-dimensional frequency parameters for all configurations and volume fractions. On the other hand, introduction of the microstructure material size effect increases the material rigidity which increases the non-dimensional frequency parameters for all values of the nonlocal parameters and volume fractions. Comparison between the considered CNT configurations shows that the largest values of the non-dimensional frequency parameters are detected with FGX -CNT nanoplates while the FGO -CNT nanoplates produce the smallest values of the non-dimensional frequency parameter. Additionally, increasing the reinforcement volume fraction increases the overall system stiffness and increases the non-dimensional frequency parameter for all CNT configurations.

The relative percentage difference of the non-dimensional frequency parameter, $\%\Delta\lambda_{e_0 a(n,m)} = 100 \times \left(\frac{\lambda_{e_0 a=0} - \lambda_{e_0 a=2}}{\lambda_{e_0 a=l_m=0}}\right)$ is significantly affected by the material length scale parameter, l_m. As shown in Table 8, increasing the material length scale parameter increases the relative percentage difference for all CNT configurations at all values of V_{TCNT} due to increasing the overall system stiffness. On the other hand, insignificant effect is observed with changing the CNT configuration and V_{TCNT}.

Dependency of the relative percentage difference of the non-dimensional frequency parameter, $\%\Delta\lambda_{lm(n,m)} = 100 \times \left(\frac{\lambda_{l_m=2} - \lambda_{l_m=0}}{\lambda_{e_0 a=l_m=0}}\right)$ on the nonlocality parameter for different CNT configurations at different values of V_{TCNT} is illustrated in Table 9. It is observed that introduction of the nonlocality effect increases the material flexibility and decreases the relative percentage difference of the non-dimensional frequency parameters for all CNT configurations at all values of V_{TCNT}. On the other hand, almost the same relative percentage difference is obtained for all CNT configurations at all values of V_{TCNT}.

5.2 Forced vibration response under moving load

The capability of the developed procedure to study and analyze the free and forced vibration behaviors of FG-CNT nanoplate under moving loads is demonstrated within this section. Consider a SSSS FG-CNT nanoplate with the following geometrical characteristics: a=100×10^{-9} m, b=a,

Table 6 Comparisons of dimensionless frequencies $\lambda_{mn} = \omega_{mn}a^2\sqrt{\rho_m/(E_m h^2)}$ of FGX -CNT nanoplates for V_{TCNT} and e_0a and $l_m\,(nm), b/a = 1, a/h = 10, and\ m = 1, n = 1$. SSSS

	$V_{TCNT} = 0.12$			$V_{TCNT} = 0.17$			$V_{TCNT} = 0.28$		
e_0a	$l_m = 0$	$l_m = 1$	$l_m = 2$	$l_m = 0$	$l_m = 1$	$l_m = 2$	$l_m = 0$	$l_m = 1$	$l_m = 2$
0	9.6383848	10.529440	12.937208	12.083556	13.200660	16.219254	14.356524	15.683754	19.270256
0.5	9.6383848	10.529440	12.937208	12.083556	13.200660	16.219254	14.356524	15.683754	19.270256
1	9.6383848	10.529440	12.937208	12.083556	13.200660	16.219254	14.356524	15.683754	19.270256
1.5	9.6383848	10.529440	12.937208	12.083556	13.200660	16.219254	14.356524	15.683754	19.270256
2	9.6383848	10.529440	12.937208	12.083556	13.200660	16.219254	14.356524	15.683754	19.270256

Table 7 Comparisons of dimensionless frequencies $\lambda_{mn} = \omega_{mn}a^2\sqrt{\rho_m/(E_m h^2)}$ of FGO -CNT nanoplates for V_{TCNT} and e_0a and $l_m\,(nm), b/a = 1, a/h = 10, and\ m = 1, n = 1$. SSSS

	$V_{TCNT} = 0.12$			$V_{TCNT} = 0.17$			$V_{TCNT} = 0.28$		
e_0a	$l_m = 0$	$l_m = 1$	$l_m = 2$	$l_m = 0$	$l_m = 1$	$l_m = 2$	$l_m = 0$	$l_m = 1$	$l_m = 2$
0	10.419436	11.382705	13.985586	12.798543	13.981762	17.178961	14.302255	15.624480	19.197325
0.5	10.293223	11.244823	13.816178	12.643513	13.812395	16.970867	14.129004	15.435224	18.964787
1	9.5376892	10.419437	12.802051	11.715461	12.798549	15.725188	13.091923	14.302261	17.572754
1.5	8.6972218	9.5012712	11.673926	10.683086	11.670734	14.339475	11.938253	13.041936	16.024229
2	7.7626128	8.4802608	10.419443	9.5350752	10.416594	12.798547	10.655363	11.640440	14.302255

Table 8 Comparisons of the relative percentage difference of the dimensionless frequencies $\%\Delta\lambda_{e_0a(n,m)}$ of nanoplates with different CNT configurations for V_{TCNT} and e_0a and $l_m\,(nm)$, $\frac{b}{a} = 1$, $a/h = 10$, $and\ m = 1, n = 1$. SSSS

	$V_{TCNT} = 0.12$			$V_{TCNT} = 0.17$			$V_{TCNT} = 0.28$		
CNT	$l_m = 0$	$l_m = 1$	$l_m = 2$	$l_m = 0$	$l_m = 1$	$l_m = 2$	$l_m = 0$	$l_m = 1$	$l_m = 2$
	$\%\Delta\lambda_{e_0a(1,1)}$			$\%\Delta\lambda_{e_0a(1,1)}$			$\%\Delta\lambda_{e_0a(1,1)}$		
UD- CNT	25.4987	27.8561	34.2258	25.49871	27.85605	34.22588	25.49871	27.85603	34.22587
FGΛ- CNT	25.4987	27.85605	34.2259	25.49871	27.85603	34.22587	25.4987	27.85607	34.22593
FGX- CNT	25.4987	27.8560	34.2259	25.4987	27.85604	34.22583	25.49901	27.85646	34.22612
FGO- CNT	25.4987	27.8561	34.2259	25.49874	27.85605	34.22588	25.49872	27.85603	34.22586

a/h=10. The nanoplate is subjected to a moving load of intensity 10^{-9} *N*. The Newmark numerical integration technique is adopted to solve the dynamic finite elements equation of motion using $\Delta t = T_{final}/500$, $T_{final} = L/v$. The dimensionless speed parameter, β is applied as $\beta = v/v_{crital}$, when β=1 means the load velocity is equal to first critical speed of the plate. The midspan displacements are normalized by using the static midpoint deflection of the plate without any CNT addition. The dynamic magnification factor is defined as, $W_{rel} = \frac{W(L/2,t)}{W_{static}(L/2)|_{k=0}}$.

The dependency of the dynamic magnification factor on the dimensionless speed parameter, β for different FG-CNT configurations at different *CNT* volume fractions is shown in Fig. 3. It is observed that, increasing the reinforcement volume fraction increases the material rigidity and decreases the dynamic magnification factors for all CNT configurations. On the other hand, comparison between the different FG-CNT configurations revealed that both FGΛ-CNT and FGX-CNT configurations increase the overall system stiffness and produce smaller values of the dynamic magnification factor compared with those obtained by FGO-CNT and UD-CNT especially at higher values of the CNT volume fractions. Additionally, FGO-CNT configuration produces more flexible CNT nanoplate and results in larger values of the dynamic magnification factors for all values of volume fractions.

Keeping constant value of the material length scale parameter, l_m, variations of the dynamic magnification factor, W_{rel} versus the dimensionless speed parameter, β at different values of the non-classical nonlocal parameter, e_0a for different FG-CNT nanoplate configurations are depicted in Fig. 4. It is revealed that introduction of thenonlocality effect increases the overall system flexibility and produces larger values of the dynamic magnification factor for all FG-CNT nanoplate configurations at all values of volume fractions. Additionally, increasing the nonlocal parameter leads to reach the maximum magnification factor at smaller value of the dimensionless speed parameter for all CNT nanoplate configurations.

The stability of the forced vibration response of FG_CNT nanoplate significantly affected by the dimension-

Table 9 Comparisons of the relative percentage difference of the dimensionless frequencies $\%\Delta\lambda_{l_m(n,m)}$ of nanoplates with different CNT configurations for V_{TCNT} and e_0a and l_m $(nm), b/a = 1, a/h = 10, and\ m = 1, n = 1$. SSSS

	$V_{TCNT} = 0.12$				$V_{TCNT} = 0.17$				$V_{TCNT} = 0.28$			
	$\%\Delta\lambda_{l_m}$				$\%\Delta\lambda_{l_m}$				$\%\Delta\lambda_{l_m}$			
e_0a	UD-CNT	FGΛ-CNT	FGX-CNT	FGO-CNT	UD-CNT	FGΛ-CNT	FGX-CNT	FGO-CNT	UD-CNT	FGΛ-CNT	FGX-CNT	FGO-CNT
0	34.2259	34.2259	34.2259	34.2259	34.2259	34.2258	34.2258	34.2259	34.226	34.226	34.2262	34.2259
0.5	33.8113	33.8113	33.8113	33.8114	33.8113	33.8113	33.8113	33.8113	33.8112	33.8114	33.8112	33.8113
1	31.3295	31.3296	31.3295	31.3295	31.3295	31.3294	31.3295	31.3296	31.3295	31.3296	31.3293	31.3295
1.5	28.5687	28.5688	28.5687	28.5688	28.5688	28.5687	28.5687	28.5688	28.5687	28.5688	28.5689	28.5688
2	25.4987	25.4988	25.4987	25.4988	25.4988	25.4986	25.4987	25.4988	25.4987	25.4988	25.4991	25.4987

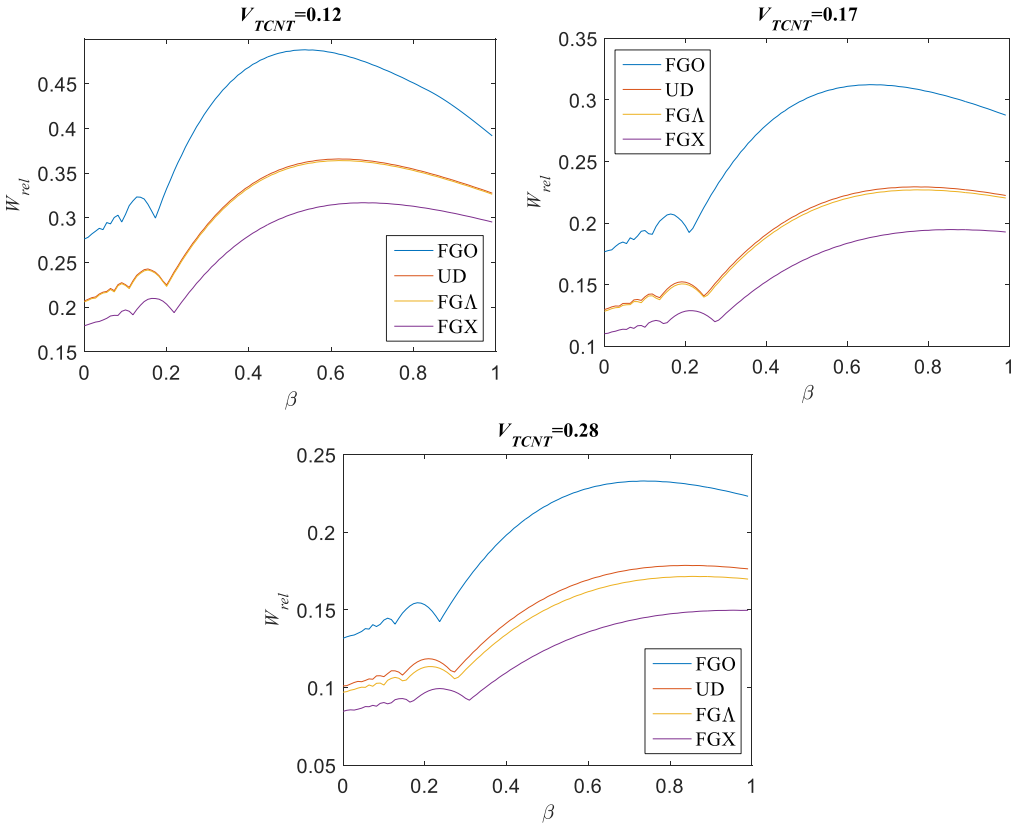

Fig. 3 Comparisons of maximum midspan deflections of UD-CNT, FGΛ-CNT, FGX-CNT and FGO-CNT nanoplates versus β for $V_{TCNT} = 0.12, 0.17, 0.28,$ power-law exponent k=1 in FGΛ-CNT, FGX-CNT and FGO-CNT

less speed parameter, β. The dynamic magnification factor profiles throughout the normalized coordinate $x_p(t)/L$ at different reinforcement volume fractions of CNT nanoplate configurations at two different values of dimensionless speed parameter, β = 0.25 and 0.5 are presented in Fig. 5. It is seen that oscillatory dynamic magnification factor profiles with are produced at smaller values of the dimensionless speed parameters, β = 0.25 due to the transient dynamic effect. Theses oscillations disappear at higher values of the dimensionless speed parameters, β = .5. Additionally, the amplitudes of these oscillations decrease with increasing the reinforcement volume fraction for all CNT nanoplate configurations due to increasing the material rigidity. Due to its high flexibility, FGO- CNT nanoplate produces dynamic magnification factor profiles with fewer number of oscillations with smaller amplitudes at β=0.25 compared with the corresponding profiles produced by other CNT nanoplates.

The dynamic magnification factor profiles throughout the normalized coordinates at different values of the nonlocality parameter for all CNT nanoplate configurations at β = 0.25 and 0.5; respectively are shown in Fig. 6. It may be noticed that incorporating the nonlocality effect increases the overall system compliance and produces oscillatory motion with larger amplitudes specially at smaller values of β for all CNT nanoplate configurations. It is also revealed that FGX-CNT produces more rigid CNT nanoplate and produces oscillatory motions with larger

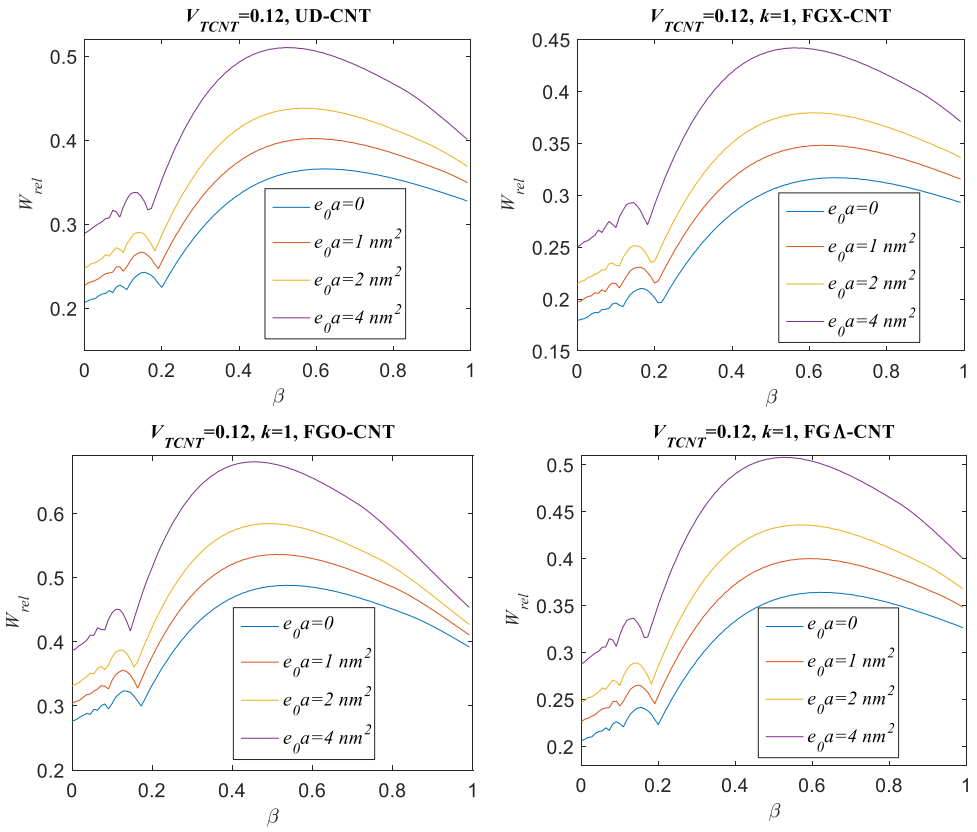

Fig. 4 Comparisons of maximum midspan deflections of UD-CNT, FGΛ-CNT, FGX-CNT and FGO-CNT nanoplates versus β for $V_{TCNT} = 0.12$. Nonlocal parameter $e_0a = 0, 1, 2 \; and \; 4 \; nm^2$. Size parameter $l_m = 0$

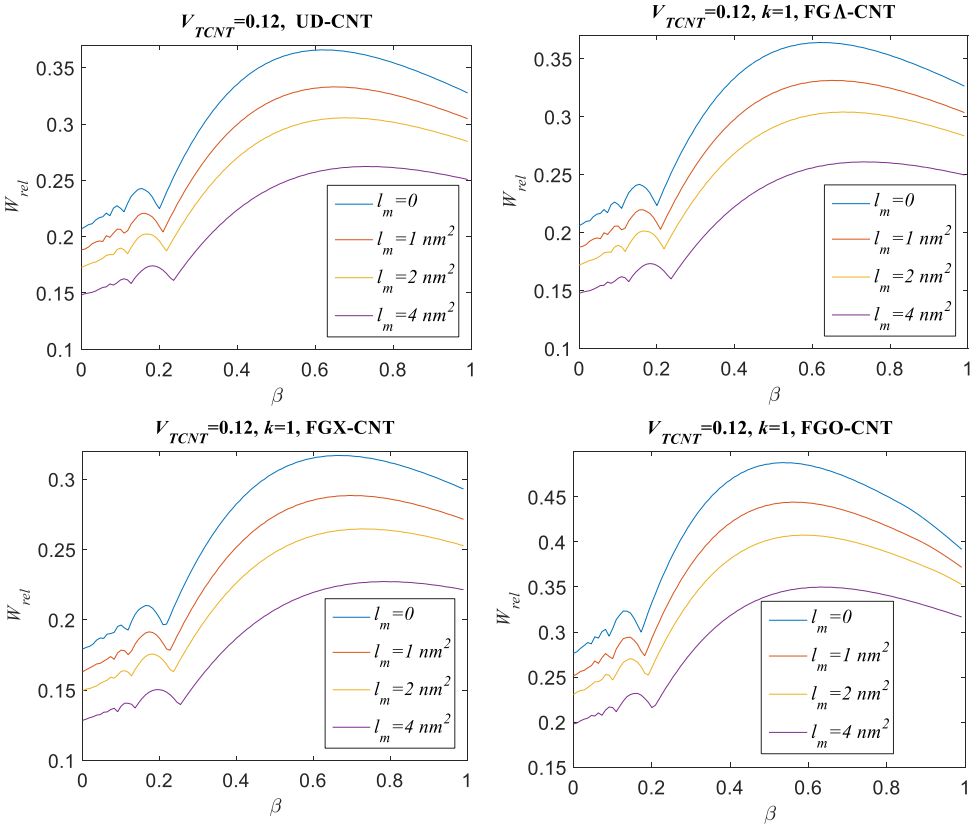

Fig. 5 Comparisons of maximum midspan deflections of UD-CNT, FGΛ-CNT, FGX-CNT and FGO-CNT nanoplates versus β for $V_{TCNT} = 0.12$. Nonlocal parameter $e_0a = 0$. Size parameter $l_m = 0, 1, 2 \; and \; 4 \; nm^2$

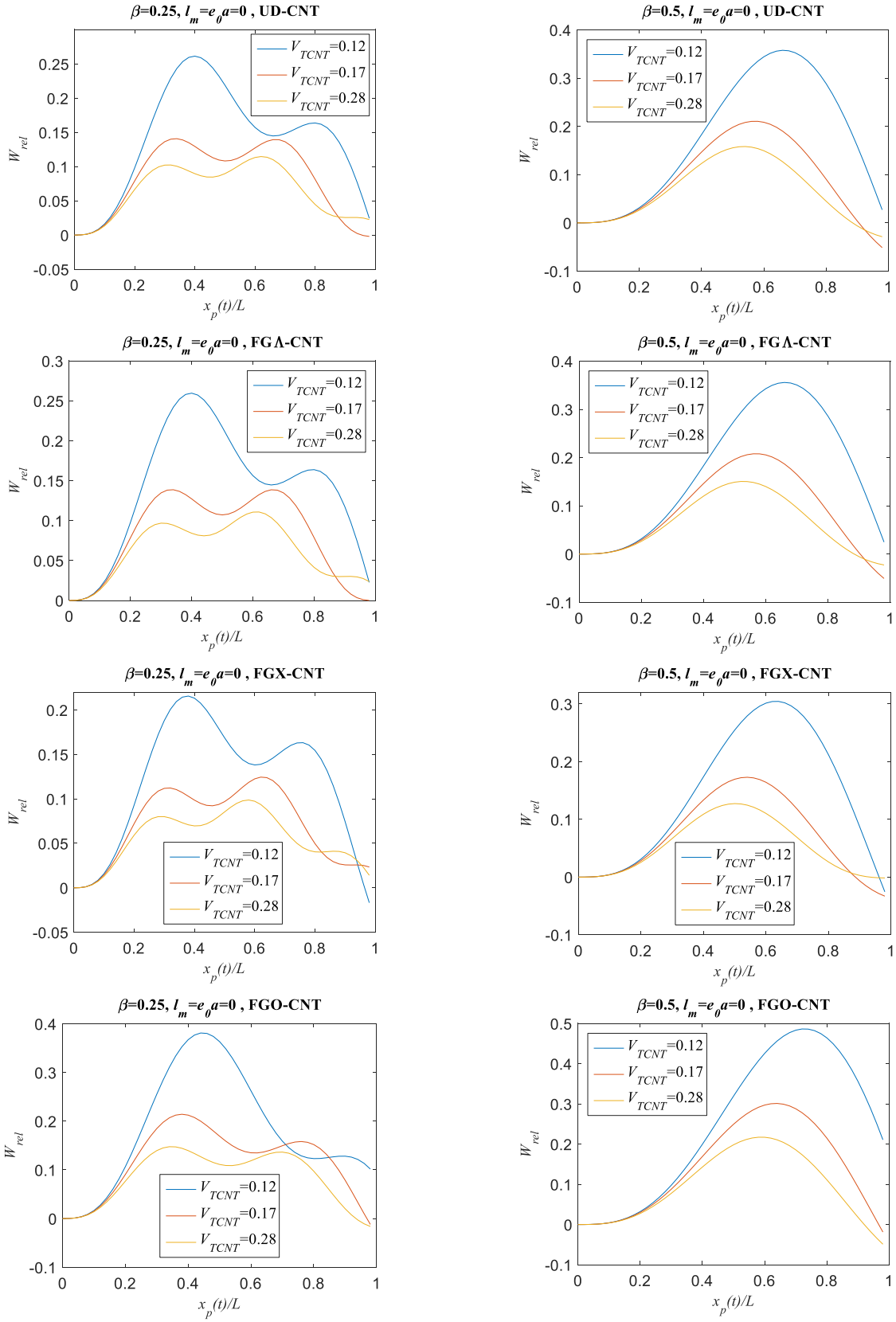

Fig. 6 Comparisons of time histories of midpoint deflections of CNT nanoplates for different distributions for β =0.25 and 0.5 and for different volume fractions, nonlocal parameter $e_0a = 0$. size parameter $l_m = 0$

number of oscillations while the FGO-CNT results in a more compliant CNT nanoplate and produces oscillatory motion with fewer number of oscillations especially at lower values of the dimensionless speed parameter, β.

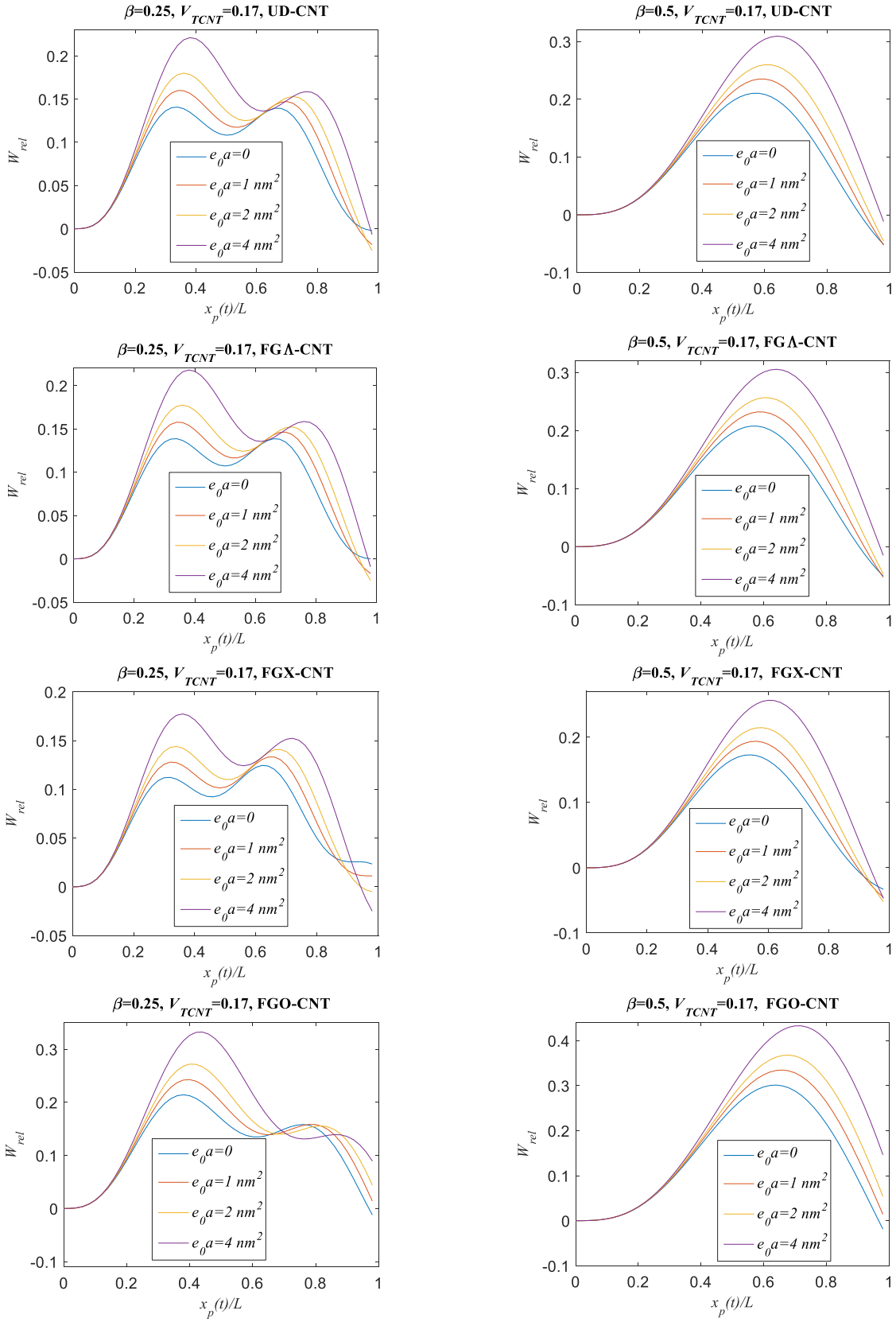

Fig. 7 Comparisons of time histories of midpoint deflections of CNT nanoplates for different distributions for β =0.25 and 0.5 and for different value of the nonlocal parameter e_0a, and size parameter $l_m = 0$

Neglecting the nonlocality effect, introducing the micro-structure size effect significantly affects the stability of the transient time response of FG-CNT nanoplate especially at low values of the dimensionless speed parameter, β. As

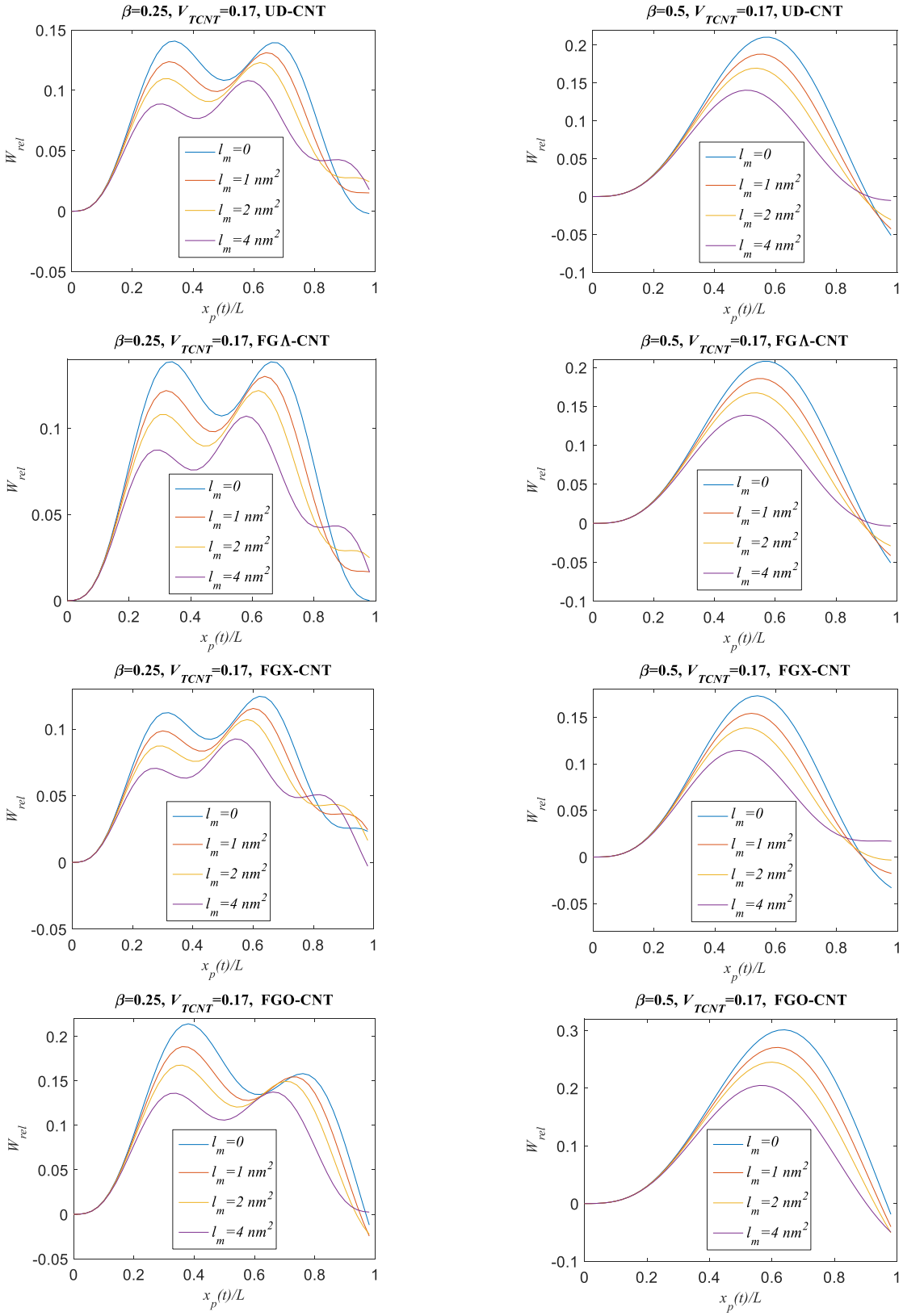

Fig. 8 Comparisons of time histories of midpoint deflections of CNT nanplates for different distributions for β =0.25 and 0.5 and for different values of the material size parameter for nonlocal parameter $e_0 a = 0$

shown in Fig. 8, at smaller values of β, magnification factor profiles are produced with larger number of oscillations are detected as the microstructure length scale parameter increases for all CNT nanoplates due to increasing the system rigidity. These oscillations disappear at higher values of β.

5. Conclusions

To consider the influence of size and microstructures scales on the dynamic responses of FG-CNT nanoplate under moving load, the nonlocal strain gradient theory has been exploited with modified continuum model. The effect of reinforcement configuration is investigated by considering four different CNT nanoplate configurations. The different distributions of CNT throughout the nanoplate thickness are considered. The dynamic motion equations with their associated boundary conditions are derived based on the Hamiltonian principle. The analytical solution is obtained using the Navier procedure. The proposed methodology is verified and compared. Based on the parametric results the following concluding remarks are drawn:

• Dynamic vibration responses (free and forced) of CNT nanoplate under moving load are dependent on the reinforcement volume fraction of CNTs, V_{TCNT}. Increasing this volume fraction increases the material rigidity thus increases the frequency parameter, λ and decreases the dynamic magnification factor W_{rel}.

• FG-CNT configuration significantly affects the dynamic behaviour of CNT nanoplate. FGX-CNT produces a more rigid nanoplate and results in higher values of the frequency parameters, λ and smaller values of the dynamic magnification factors, W_{rel}.

• On the other hand a more compliant nanoplate is obtained by FGO-CNT configuration which produces smaller values of the non-dimensional frequency parameters λ and larger values of the dynamic magnification factor, $W_{rel.}$.

• Dynamic responses under moving load are greatly affected by the non-classical nonlocal and material size parameters.

• Incorporation of the nonlocality parameter increases the material compliance and produces smaller values of the non-dimensional frequency parameter and larger values of the dynamic magnification factor.

• On the other hand, introduction of the material size parameter produces rigid nanoplates thus larger values of the non-dimensional frequency parameters and smaller values of the dynamic magnification factors are produced.

• The stability of the dynamic time response of FG-CNT nanoplates under moving load could be controlled by the dimensionless speed parameter, β. Profiles with fewer oscillations are obtained at higher values of β.

• The proposed model and the obtained numerical results are supportive for the design and manufacturing of such FGCNT nanoplate for several applications.

Acknowledgments

The authors extend their appreciation to the Deputyship for Research & Innovation, Ministry of Education in Saudi Arabia for funding this research work through the project number ISP23-49.

References

Abdelrahman, A.A., Esen, I., Ozarpa, C., Shaltout, R., Eltaher, M.A. and Assie, A.E. (2021a), "Dynamics of perforated higher order nanobeams subject to moving load using the nonlocal strain gradient theory", *Smart Struct. Syst.*, **28**(4), 515-533. https://doi.org/10.12989/sss.2021.28.4.515

Abdelrahman, A.A., Esen, I., Daikh, A.A. and Eltaher, M.A. (2021b), "Dynamic analysis of FG nanobeam reinforced by carbon nanotubes and resting on elastic foundation under moving load", *Mech. Based Des. Struct.*, 1-24. https://doi.org/10.1080/15397734.2021.1999263

Abdelrahman, A., Shanab, R.A., Esen, I. and Eltaher, M.A. (2022), "Effect of moving load on dynamics of nanoscale Timoshenko CNTs embedded in elastic media based on doublet mechanics theory", *Steel Compos. Struct.*, **44**(2), 255. https://doi.org/10.12989/scs.2022.44.2.255

Alazwari, M.A., Daikh, A.A. and Eltaher, M.A. (2022), "Novel quasi 3D theory for mechanical responses of FG-CNTs reinforced composite nanoplates", *Adv. Nano Res.*, **12**(2), 117. https://doi.org/10.12989/anr.2022.12.2.117

Alshorbagy, A.E., Eltaher, M.A. and Mahmoud, F. (2011), "Free vibration characteristics of a functionally graded beam by finite element method", *Appl. Math. Modell.*, **35**(1), 412-425. https://doi.org/10.1016/j.apm.2010.07.006

Ansari, R., Shahabodini, A. and Shojaei, M.F. (2016), "Vibrational analysis of carbon nanotube-reinforced composite quadrilateral plates subjected to thermal environments using a weak formulation of elasticity", *Compos. Struct.*, **139**, 167-187. https://doi.org/10.1016/j.compstruct.2015.11.079

Assie, A., Akbaş, Ş.D., Bashiri, A.H., Abdelrahman, A.A. and Eltaher, M.A. (2021), "Vibration response of perforated thick beam under moving load", *Eur. Phys. J. Plus*, **136**(3), 1-15. https://doi.org/10.1140/epjp/s13360-021-01224-2

Barati, M.R. (2017), "Nonlocal-strain gradient forced vibration analysis of metal foam nanoplates with uniform and graded porosities", *Adv. Nano Res.*, **5**(4), 393. https://doi.org/10.12989/anr.2017.5.4.393

Bouafia, H., Chikh, A., Bousahla, A. A., Bourada, F., Heireche, H., Tounsi, A., Benrahou, K.H., Tounsi, A., Al-Zahrani, M.M. and Hussain, M. (2021), "Natural frequencies of FGM nano-plates embedded in an elastic medium", *Adv. Nano Res.*, **11**(3), 239. https://doi.org/10.12989/anr.2021.11.3.239

Daikh, A.A., Belarbi, M.O., Salami, S.J., Ladmek, M., Belkacem, A., Houari, M.S.A., Ahmed, H.M. and Eltaher, M.A. (2023), "A three-unknown refined shear beam model for the bending of randomly oriented FG-CNT/fiber-reinforced composite laminated beams rested on a new variable elastic foundation", *Acta Mechanica*, **234**(10), 5171-5186. https://doi.org/10.1007/s00707-023-03657-5

Ding, H.X. and She, G.L. (2021), "A higher-order beam model for the snap-buckling analysis of FG pipes conveying fluid", *Struct. Eng. Mech.*, **80**(1), 63-72. http://doi.org/10.12989/sem.2021.80.1.063.

Drai, A., Daikh, A.A., Belarbi, M.O., Houari, M.S.A., Aour, B., Hamdi, A. and Eltaher, M.A. (2023), "Bending of axially functionally graded carbon nanotubes reinforced composite nanobeams", *Adv. Nano Res.*, **14**(3), 211. https://doi.org/10.12989/anr.2023.14.3.211

Eltaher, M.A., Abdelrahman, A.A. and Esen, I. (2021), "Dynamic analysis of nanoscale Timoshenko CNTs based on doublet mechanics under moving load", *Eur. Phys. J. Plus*, **136**(7), 1-21. https://doi.org/10.1140/epjp/s13360-021-01682-8

Esen, I., Abdelrahman, A.A. and Eltaher, M.A. (2020), "Dynamics analysis of timoshenko perforated microbeams under moving loads", *Eng. Comput.*, 1-17. https://doi.org/10.1007/s00366-020-01212-7

Esen, I., Daikh, A.A. and Eltaher, M.A. (2021a), "Dynamic response of nonlocal strain gradient FG nanobeam reinforced by carbon nanotubes under moving point load", *Eur. Phys. J. Plus*,

136(4), 1-22. https://doi.org/10.1140/epjp/s13360-021-01419-7

Esen, I., Abdelrahman, A.A. and Eltaher, M.A. (2021b), "On vibration of sigmoid/symmetric functionally graded nonlocal strain gradient nanobeams under moving load", *Int. J. Mech. Mater. Des.*, 1-22. https://doi.org/10.1007/s10999-021-09555-9

Farahmand, H. (2021), "A variational approach for analytical buckling solution of moderately thick microplate using strain gradient theory incorporating two-variable refined plate theory: a benchmark study", *J. Brazil. Soc. Mech. Sci. Eng.*, **43**(3), 1-11. https://doi.org/10.1007/s40430-020-02766-9

Farzam, A. and Hassani, B. (2018), "Thermal and mechanical buckling analysis of FG carbon nanotube reinforced composite plates using modified couple stress theory and isogeometric approach", *Compos. Struct.*, **206**, 774-790. https://doi.org/10.1016/j.compstruct.2018.08.030

Ghorbanpour Arani, A., Rousta Navi, B. and Mohammadimehr, M. (2016), "Surface stress and agglomeration effects on nonlocal biaxial buckling polymeric nanocomposite plate reinforced by CNT using various approaches", *Adv. Compos. Mater.*, **25**(5), 423-441. https://doi.org/10.1080/09243046.2015.1052189

Griebel, M. and Hamaekers, J. (2004), "Molecular dynamics simulations of the elastic moduli of polymer–carbon nanotube composites", *Comput. Meth. Appl. Mech. Eng.*, **193**(17-20), 1773-1788. https://doi.org/https://doi.org/10.1016/j.cma.2003.12.025

Han, Y. and Elliott, J. (2007), "Molecular dynamics simulations of the elastic properties of polymer/carbon nanotube composites", *Comput. Mater. Sci.*, **39**(2), 315-323. https://doi.org/10.1016/j.commatsci.2006.06.011

Karami, B. and Karami, S. (2019), "Buckling analysis of nanoplate-type temperature-dependent heterogeneous materials", *Adv. Nano Res.*, **7**(1), 51. https://doi.org/10.12989/anr.2019.7.1.051

Ke, L.L., Yang, J. and Kitipornchai, S. (2010), "Nonlinear free vibration of functionally graded carbon nanotube-reinforced composite beams", *Compos. Struct.*, **92**(3), 676-683. https://doi.org/https://doi.org/10.1016/j.compstruct.2009.09.024

Kolahdouzan, F., Mosayyebi, M., Ghasemi, F.A., Kolahchi, R. and Panah, S.R.M. (2020), "Free vibration and buckling analysis of elastically restrained FG-CNTRC sandwich annular nanoplates", *Adv. Nano Res.*, **9**(4), 237-250. https://doi.org/10.12989/anr.2020.9.4.237

Lei, Z. X., Liew, K. M. and Yu, J. L. (2013), "Buckling analysis of functionally graded carbon nanotube-reinforced composite plates using the element-free kp-Ritz method", *Compos. Struct.*, **98**, 160-168. https://doi.org/10.1016/j.compstruct.2012.11.006.

Liew, K.M., Lei, Z.X., Yu, J.L. and Zhang, L. (2014), "Postbuckling of carbon nanotube-reinforced functionally graded cylindrical panels under axial compression using a meshless approach", *Comput. Meth. Appl. Mech. Eng.*, **268**, 1-17. https://doi.org/10.1016/j.cma.2013.09.001

Lim, C.W., Zhang, G. and Reddy, J. (2015), "A higher-order nonlocal elasticity and strain gradient theory and its applications in wave propagation", *J. Mech. Phys. Solids*, **78**, 298-313. https://doi.org/10.1016/j.jmps.2015.02.001

Lin, F. and Xiang, Y. (2014), "Vibration of carbon nanotube reinforced composite beams based on the first and third order beam theories", *Appl. Math. Modell.*, **38**(15-16), 3741-3754. https://doi.org/10.1016/j.apm.2014.02.008

Liu, H., Zhang, Q., Yang, X. and Ma, J. (2021), "Size-dependent vibration of laminated composite nanoplate with piezo-magnetic face sheets", *Eng. Comput.*, 1-17. https://doi.org/10.1007/s00366-021-01285-y

Lu, L., She, G.L., and Guo, X. (2021), "Size-dependent post-buckling analysis of graphene reinforced composite microtubes with geometrical imperfection", *Int. J. Mech. Sci.*, **199**, 106428. https://doi.org/10.1016/j.ijmecsci.2021.106428.

Iijima, S. (1991), "Helical microtubules of graphitic carbon", *Nature*, **354**(6348), 56-58.

Mahesh, V. and Harursampath, D. (2020), "Nonlinear deflection analysis of CNT/magneto-electro-elastic smart shells under multi-physics loading", *Mech. Adv. Mater. Struct.*, **1-25**. https://doi.org/10.1080/15376494.2020.1805059

Mirzaei, M. and Kiani, Y. (2015), "Thermal buckling of temperature dependent FG-CNT reinforced composite conical shells", *Aerosp. Sci. Technol.*, **47**, 42-53.

Mirzaei, M. and Kiani, Y. (2016), "Thermal buckling of temperature dependent FG-CNT reinforced composite plates", *Meccanica*, **51**(9), 2185-2201.

Mohammadimehr, M., Arshid, E., Alhosseini, S.M.A.R., Amir, S. and Arani, M.R.G. (2019), "Free vibration analysis of thick cylindrical MEE composite shells reinforced CNTs with temperature-dependent properties resting on viscoelastic foundation", *Struct. Eng. Mech.*, **70**(6), 683-702. https://doi.org/10.12989/sem.2019.70.6.683

Mohammadimehr, M. and Mostafavifar, M. (2016), "Free vibration analysis of sandwich plate with a transversely flexible core and FG-CNTs reinforced nanocomposite face sheets subjected to magnetic field and temperature-dependent material properties using SGT", *Compos. Part B Eng.*, **94**, 253-270. https://doi.org/10.1016/j.compositesb.2016.03.030

Mohammadimehr, M., Navi, B.R. and Arani, A.G. (2015), "Free vibration of viscoelastic double-bonded polymeric nano-composite plates reinforced by FG-SWCNTs using MSGT, sinusoidal shear deformation theory and meshless method", *Compos. Struct.*, **131**, 654-671. https://doi.org/10.1016/j.compstruct.2015.05.077

Mohammadimehr, M., Salemi, M. and Navi, B.R. (2016a), "Bending, buckling, and free vibration analysis of MSGT microcomposite Reddy plate reinforced by FG-SWCNTs with temperature-dependent material properties under hydro-thermo-mechanical loadings using DQM", *Compos. Struct.*, **138**, 361-380. https://doi.org/10.1016/j.compstruct.2015.11.055

Mohammadimehr, M., Navi, B.R. and Arani, A.G. (2016b), "Modified strain gradient Reddy rectangular plate model for biaxial buckling and bending analysis of double-coupled piezoelectric polymeric nanocomposite reinforced by FG-SWNT", *Compos. Part B Eng.*, **87**, 132-148. https://doi.org/10.1016/j.compositesb.2015.10.007

Mohammadimehr, M., Navi, B.R. and Arani, A.G. (2017), "Dynamic stability of MSGT sinusoidal viscoelastic piezo-electric polymeric FG-SWNT reinforced nanocomposite plate considering surface stress and agglomeration effects under hydro-thermo-electro-magneto-mechanical loadings", *Mech. Adv. Mater. Struct*, **24**(16), 1325-1342. http://doi.org/10.1080/15376494.2016.1227507

Nguyen, H.X., Nguyen, T.N., Abdel-Wahab, M., Bordas, S.P., Nguyen-Xuan, H. and Vo, T.P. (2017), "A refined quasi-3D isogeometric analysis for functionally graded microplates based on the modified couple stress theory", *Comput. Meth. Appl. Mech. Eng.*, **313**, 904-940. https://doi.org/10.1016/j.cma.2016.10.002

Phung-Van, P., Abdel-Wahab, M., Liew, K.M., Bordas, S.P.A. and Nguyen-Xuan, H. (2015), "Isogeometric analysis of functionally graded carbon nanotube-reinforced composite plates using higher-order shear deformation theory", *Compos. Struct.*, **123**, 137-149. https://doi.org/10.1016/j.compstruct.2014.12.021

Phung-Van, P., Lieu, Q.X., Nguyen-Xuan, H. and Wahab, M.A. (2017), "Size-dependent isogeometric analysis of functionally graded carbon nanotube-reinforced composite nanoplates", *Compos. Struct.*, **166**, 120-135. http://doi.org/10.1016/j.compstruct.2017.01.049.

Rafiee, M., He, X.Q. and Liew, K.M. (2014), "Non-linear dynamic stability of piezoelectric functionally graded carbon nanotube-reinforced composite plates with initial geometric imperfection", *Int. J. Non-Linear Mech.*, **59**, 37-51. https://doi.org/10.1016/j.ijnonlinmec.2013.10.011

Reddy, J.N. (2003), *Mechanics of Laminated Composite Plates and Shells*: *Theory and Analysis*, CRC press.

Reddy, J. (2007), "Nonlocal theories for bending, buckling and vibration of beams", *Int. J. Eng. Sci.*, **45**(2-8), 288-307. https://doi.org/10.1016/j.ijengsci.2007.04.004

Salari, E., Ashoori, A. and Vanini, S.A.S. (2019), "Porosity-dependent asymmetric thermal buckling of inhomogeneous annular nanoplates resting on elastic substrate", *Adv. Nano Res.*, **7**(1), 25. https://doi.org/10.12989/anr.2019.7.1.025

She, G.L. (2021), "Guided wave propagation of porous functionally graded plates: The effect of thermal loadings", *J. Therm. Stresses*, **44**(10), 1289-1305. https://doi.org/10.1080/01495739.2021.1974323

She, G.L., Liu, H.B., and Karami, B. (2021), "Resonance analysis of composite curved microbeams reinforced with graphene nanoplatelets", *Thin Wall. Struct.*, **160**, 107407. https://doi.org/10.1016/j.tws.2020.107407

Shen, H.S. (2009), "Nonlinear bending of functionally graded carbon nanotube-reinforced composite plates in thermal environments", *Compos. Struct.*, **91**(1), 9-19. https://doi.org/10.1016/j.compstruct.2009.04.026

Shen, H.S. (2011), "Postbuckling of nanotube-reinforced composite cylindrical shells in thermal environments, Part I: Axially-loaded shells", *Compos. Struct.*, **93**(8), 2096-2108.

Shen, H.S. and Zhang, C.L. (2010), "Thermal buckling and postbuckling behavior of functionally graded carbon nanotube-reinforced composite plates", *Mater. Des.*, **31**(7), 3403-3411. https://doi.org/10.1016/j.matdes.2010.01.048

Shen, H.S. and Xiang, Y. (2012), "Nonlinear vibration of nanotube-reinforced composite cylindrical shells in thermal environments", *Comput. Meth. Appl. Mech. Eng.*, **213**, 196-205. https://doi.org/10.1016/j.compstruct.2011.02.011

Shen, H.S. and Zhu, Z. (2012), "Postbuckling of sandwich plates with nanotube-reinforced composite face sheets resting on elastic foundations", *Eur. J. Mech. A Solids*, **35**, 10-21. https://doi.org/10.1016/j.euromechsol.2012.01.005

Shen, H.S. and Xiang, Y. (2013), "Nonlinear analysis of nanotube-reinforced composite beams resting on elastic foundations in thermal environments", *Eng. Struct.*, **56**, 698-708. https://doi.org/10.1016/j.engstruct.2013.06.002

Shen, H.S. and Xiang, Y. (2014), "Nonlinear bending of nanotube-reinforced composite cylindrical panels resting on elastic foundations in thermal environments", *Eng. Struct.*, **80**, 163-172. https://doi.org/10.1016/j.engstruct.2014.08.038

Thai, C.H., Ferreira, A.J.M., Nguyen-Xuan, H., Nguyen, L.B. and Phung-Van, P. (2021), "A nonlocal strain gradient analysis of laminated composites and sandwich nanoplates using meshfree approach", *Eng. Comput.*, 1-17. https://doi.org/10.1007/s00366-021-01501-9

Tharwan, M.Y., Daikh, A.A., Assie, A.E., Alnujaie, A. and Eltaher, M.A. (2023), "Refined quasi-3D shear deformation theory for buckling analysis of functionally graded curved nanobeam rested on Winkler/Pasternak/Kerr foundation", *Mech. Based Des. Struct. Mach.*, 1-24. https://doi.org/10.1080/15397734.2023.2270043

Wattanasakulpong, N. and Ungbhakorn, V. (2013), "Analytical solutions for bending, buckling and vibration responses of carbon nanotube-reinforced composite beams resting on elastic foundation", *Comput. Mater. Sci.*, **71**, 201-208. https://doi.org/10.1016/j.commatsci.2013.01.028

Xu, C., Qu, J., Rong, D., Zhou, Z. and Leung, A.Y.T. (2021), "Theory and modeling of a novel class of nanoplate-based mass sensors with corner point supports", *Thin Wall. Struct.*, **159**, 107306. https://doi.org/10.1016/j.tws.2020.107306

Yas, M.H. and Samadi, N. (2012), "Free vibrations and buckling analysis of carbon nanotube-reinforced composite Timoshenko beams on elastic foundation", *Int. J. Press. Vess. Pip.*, **98**, 119-128. https://doi.org/10.1016/j.ijpvp.2012.07.012

Zhang, L.W., Liew, K.M. and Reddy, J. (2016), "Postbuckling of carbon nanotube reinforced functionally graded plates with edges elastically restrained against translation and rotation under axial compression", *Comput. Meth. Appl. Mech. Eng.*, **298**, 1-28. https://doi.org/10.1016/j.cma.2015.09.016

Zhang, L.W. and Liew, K.M. (2015), "Geometrically nonlinear large deformation analysis of functionally graded carbon nanotube reinforced composite straight-sided quadrilateral plates", *Comput. Meth. Appl. Mech. Eng.*, **295**, 219-239. https://doi.org/10.1016/j.cma.2015.07.006

Zhang, L.W., Song, Z.G. and Liew, K.M. (2015), "State-space Levy method for vibration analysis of FG-CNT composite plates subjected to in-plane loads based on higher-order shear deformation theory", *Compos. Struct.*, **134**, 989-1003. https://doi.org/10.1016/j.compstruct.2015.08.138

Zhang, Y.Y., Wang, Y.X., Zhang, X., Shen, H.M., and She, G.L., (2021), "On snap-buckling of FGCNTR curved nanobeams considering surface effects", *Steel Compos. Struct.*, **38**(3), 293-304. http://doi.org/10.12989/scs.2021.38.3.293

Zhang, Y.W., She, G.L. and Eltaher, M.A. (2023), "Nonlinear transient response of graphene platelets reinforced metal foams annular plate considering rotating motion and initial geometric imperfection", *Aerosp. Sci. Technol.*, **142**, 108693. https://doi.org/10.1016/j.ast.2023.108693

Zhu, P., Lei, Z.X. and Liew, K.M. (2012a), "Static and free vibration analyses of carbon nanotube-reinforced composite plates using finite element method with first order shear deformation plate theory", *Compos. Struct.*, **94**(4), 1450-1460. https://doi.org/10.1016/j.compstruct.2011.11.010

Zhu, P., Lei, Z.X. and Liew, K.M. (2012b), "Static and free vibration analyses of carbon nanotube-reinforced composite plates using finite element method with first order shear deformation plate theory", *Compos. Struct.*, **94**(4), 1450-1460. https://doi.org/10.1016/j.compstruct.2011.11.010

CC